Next Generation Anodes for Lithium-Ion Batteries

First Quarter Progress Report 2018

Dennis Dees, Point-of-Contact
Argonne National Laboratory
9700 South Cass Avenue
Argonne, IL 60439
Phone: (630) 252-7349
E-mail: dees@anl.gov

Brian Cunningham, DOE-EERE-VTO Technology Manager
U.S. Department of Energy, Battery R&D
Phone: (202) 287-5686
E-mail: brian.cunningham@ee.doe.gov

Table of Contents

Overview (page 2)

1. Research Facilities Support (page 5)
    - CAMP Facility Support Activities (ANL) (page 5)
    - Proposed Mechanism for the Gassing of Si in Water Slurries (ORNL) (page 7)
    - Thermodynamic Understanding and Abuse Performance (SNL) (page 9)
2. Characterization, Diagnostics, and Analysis (page 11)
    - Electrode heterogeneity after processing (ORNL) (page 11)
    - EQCM Studies of Silicon Anodes (ANL) (page 12)
    - Synthesis and electrochemical performance of Li2SiO3-coated silicon nanoparticles (ANL) (page 14)
    - Calendar-life versus Cycle-life aging of Lithium-ion Cells with Silicon-Graphite Composite Electrodes – Electrochemistry Data (ANL) (page 17)
3. Materials Advancements (page 19)
    - High-Performance Polymer Binders for Silicon Anode in Lithium-ion Batteries (ORNL) (page 19)
    - Lithiation Effect of the Poly(Acrylic Acid) Binders on the Silicon Anode of Lithium-Ion Batteries (ANL) (page 21)
    - Probe the relationships between functional electrolytes structure and SEI property for Si materials (LBNL) (page 23)
    - Silicon Surface Modification Using Molecular Layer Deposition (NREL) (page 25)
    - Interfacial Modification of Si Anode for High Energy Li-ion Battery (ANL) (page 27)
    - Development of High Energy Metals (LBNL) (page 30)
    - Si anodes with extended cycle life and calendar life (PNNL) (page 32)
    - Hydro/Solvothermal Synthesis and Scale-up of Silicon and Silicon-containing Nanoparticles (ANL) (page 34)
    - Lithium Inventory (ANL) (page 36)

Silicon Deep Dive Overview

Project Introduction

Silicon has received significant attention as a viable alternative to graphitic carbon as the negative electrode in lithium-ion batteries due to its high capacity and availability [1]. Elemental silicon can theoretically store >3500 mAh/g, nearly an order of magnitude higher than graphite (372 mAh/g and 818 mAh/mL, respectively). However, several problems have been identified that limit its utility including large crystallographic expansion (~320%) upon lithiation which translates to particle cracking, particle isolation, and electrode delamination issues. Further, there are fundamental and volume change related SEI stability issues, which affect cycling efficiency. The wealth of previous studies in this area is both a testament to its potential and the size of the challenge that must be overcome, requiring a great amount of innovation on multiple fronts.

BatPaC [2], a techno-economic program designed to model lithium-ion battery performance and cost, was utilized to establish program relevance by connecting DOE/USABC pack performance targets to anode targets. Generally, research with silicon containing anodes is focused on improving the specific capacity of graphite. However, this simple metric requires a more detailed analysis with factors such as the impact on average cell voltage, and volumetric capacity. It is notoriously difficult to select appropriate metrics that will enable an accurate calculation of the energy of a single electrode. Most methods estimate the volumetric energy density of active materials with the simplistic assumption that bulk density of the electrode does not undergo change in volume during cycling. While this serves well for most cathodes where the voltage can be fixed against lithium it is inappropriate for electrodes such as silicon.

As shown in Figure 1 (left frame), BatPaC calculations indicate anode volumetric capacities greater than 1000 mAh/cm^3 ($= \rho \cdot \varepsilon \cdot Q$ [$g/cm^3_{act} \cdot cm^3_{act}/cm^3_{elect} \cdot mAh/g$]) generally minimizes battery cost with an advanced NMC cathode. Note that higher capacities result in diminishing savings in cost. The analysis (right frame) also predicts that silicon-graphite electrodes with less than 75 wt% graphite can achieve the target. Finally, alloys of inactive metals (not shown) with silicon (or tin) can meet the volumetric capacity target as long as the metal choice is inexpensive (e.g. iron rather than nickel or cobalt).

Next Generation Anodes for Lithium-Ion Batteries, also referred to as the Silicon Deep Dive Program, is a five National Laboratory consortium assembled to tackle the barriers associated with development of an advanced lithium-ion negative electrode based upon silicon as the active material. This research program baselines promising silicon materials that can be developed or obtained in quantities sufficient for electrode preparation within the consortium facilities. Composite electrode and full cell development leverages recent investments made by DOE-EERE-VTO in electrode materials and characterization. The primary objective of this program is to understand and eliminate the barriers to implementation of a silicon based anode in lithium-ion cells. The Labs are focused on a single program with continuous interaction, clear protocols for analysis, and targets for developing both the understanding and cell chemistry associated with advance negative electrodes for lithium-ion cells. First and foremost, this undertaking is a full electrode/full cell chemistry project leveraging baseline electrodes prepared at the consortium facilities. All efforts are directed to understanding and developing the chemistry needed for advancing silicon-based anodes operating in full cells. Materials development efforts include active material development, binder synthesis, coatings, safety, and electrolyte additives. Efforts include diagnostic research from all partners, which span a wide range of electrochemical, chemical and structural characterization of the system across length- and time-scales. Specialized characterization techniques developed with DOE-EERE-VTO funding, include neutrons, NMR, optical, and X-ray techniques being employed to understand operation and failure mechanisms in silicon-based anodes. In addition, several strategies to mitigate lithium loss are being assessed. The project is managed as a single team effort spanning the Labs, with consensus decisions driving research directions and toward development of high-energy density lithium-ion batteries.

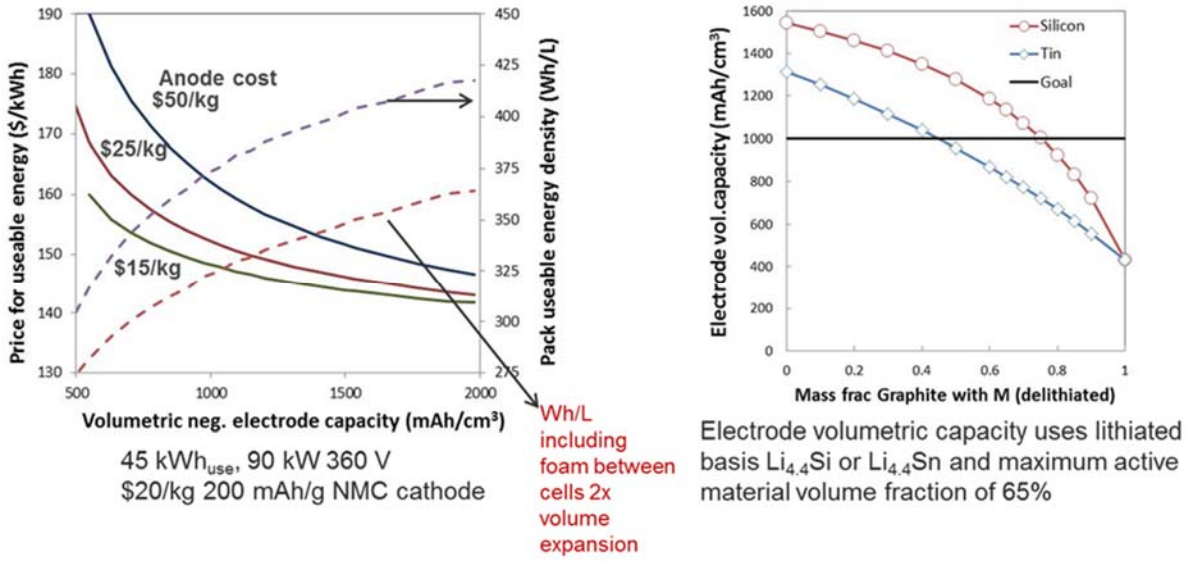

Figure 1. Battery Performance and Cost (BatPaC) model utilized to establish relevance by connecting pack to anode targets.

Objectives

- Understand and overcome the science and technology barriers to the use of silicon-based anodes in high-energy density lithium-ion batteries for transportation applications.
  - Stabilize the SEI
  - Stabilize the electrode
- Demonstrate functional prototype lithium-ion cell chemistries which meet the DOE/USABC performance targets.

Approach

Sandia National Laboratories (SNL), Oak Ridge National Laboratory (ORNL), National Renewable Energy laboratory (NREL), Lawrence Berkeley National Laboratory (LBNL), and Argonne National Laboratory (ANL) have teamed together to form an integrated program. Technical targets have been developed and regular communications have been established. Throughout the program, there is a planned focus on understanding, insights into, and advancement of silicon-based materials, electrodes, and cells. All anode advancements will be verified based on life and performance of full cells. Toward that end, baseline silicon-based materials, electrodes, and cells have been adopted, along with full cell testing protocols.

In examining improvements, changes to the baseline cell technology will be minimized. As an example, silicon active material coating improvements will be verified on baseline silicon materials in electrodes fabricated by the battery research facilities. All other components in the prototype cells (i.e. positive electrode, separator, electrolyte …) will be from the baseline technology. There are many testing protocols that can be utilized to benchmark the baseline technology. This program has adopted a testing protocol from the literature [3] that has worked well for lithium-ion cells with silicon containing anodes. Shown pictorially in Figure 2 the test starts with three slow (C/20) formation cycles, an HPPC cycle, and then the C/3 aging cycles. The test ends with another HPPC cycle and threes more slow (C/20) cycles. All constant current cycling is symmetric between charge and discharge rates. The tests are run at 30°C. If there is little or no aging in the first 100 cycles, the protocol can be repeated. This protocol effectively examines capacity, impedance, and aging effects in about a month's worth of testing.

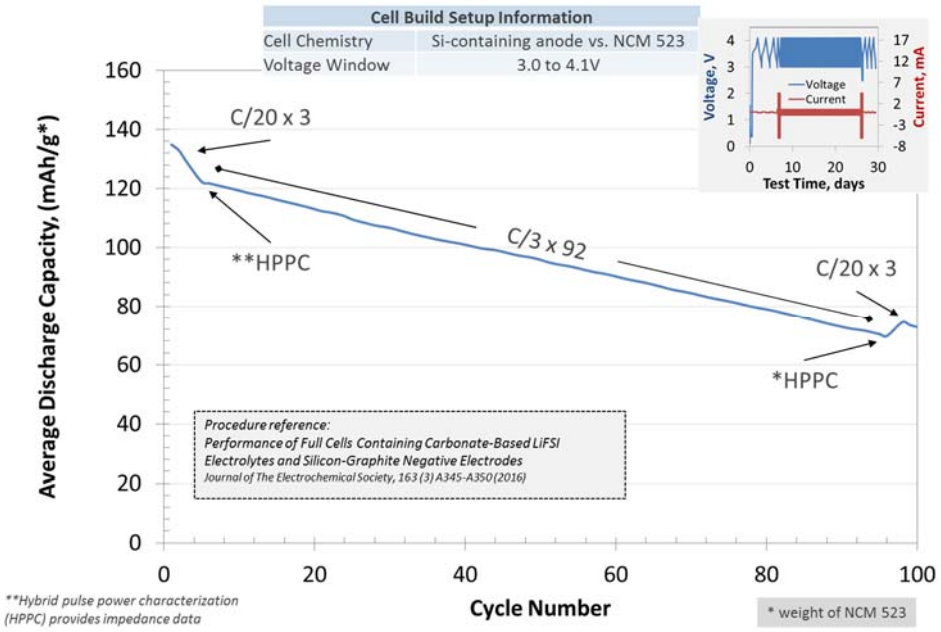

Figure 2. Full cell testing protocol.

As the program matures, materials developments will be incorporated into baseline silicon-based materials, electrodes, and cells. Scale-up of materials, incorporation of materials advancements into electrodes and prototype cells, and characterization and testing of cells, as well as evaluation of safety and abuse tolerance are part of a wide range of integrated studies supported by battery research facilities at the National Labs working closely with the program. These research facilities include the Battery Abuse Testing Laboratory (BATLab), the Battery Manufacturing Facility (BMF), the Cell Analysis, Modeling, and Prototyping (CAMP), the Materials Engineering Research Facility (MERF), and the Post-Test Facility (PTF).

The fundamental understanding of silicon-based electrode active materials is based on extensive electrochemical and analytical diagnostic studies on components, electrodes, and cells conducted within the program. This effort contains in-situ and ex-situ studies on full and specialty cells, including reference electrode cells. Overall, the diagnostic studies are intended to help establish structure-composition-property relationships, including lithium-alloying surface and bulk transport and kinetic phenomena. Further, they should form the basis for accurately assessing component and electrode failure modes and lay a path for advancements.

Supported by the diagnostic studies, materials development on silicon-based materials, electrodes, and cells is being conducted to enhance interfacial stability, accommodate intermetallic volume changes, and improve overall performance and life. Key to this effort is the development and testing of coatings and additives designed to modify and stabilize the dynamic silicon-electrolyte interface. Further, functional polymer binders designed to accommodate volume changes, increase conductivity, and improve adherence are being developed and analyzed. Finally, the program is exploring active material development. Alternative high-energy silicon-alloy/composite materials are being considered. Also, strategies for introducing additional lithium inventory into the cell are being developed.

Communication of programmatic progress to battery community is critical. This will generally be accomplished through publications, presentations, reports, and reviews. Further, the program is open to industrial participation and/or collaboration that does not limit program innovation or the free flow of information. Finally, this program is highly integrated with our sister program on SEI-Stabilization, called SEI-Sta for short. In general, SEI-Sta is focused on the development and characterization of model systems, thin-film well-defined active area electrodes on which it is easier to extract fundamental information on lithium-silicon phase formation, lithium transport, and interfacial phenomena (e.g. SEI formation and growth).

References

1. *Alloy Negative Electrodes for Li-Ion Batteries*. M.N. Obrovac and V.L. Chevrier, Chem, Rev. 2014, 114, 11444-11503.
2. *Modeling the Performance and Cost of Lithium-Ion Batteries for Electric-Drive Vehicles*. Second Edition, Argonne National Laboratory Report, ANL-12/55.
3. *Performance of Full Cells Containing Carbonate-Based LiFSI Electrolytes and Silicon-Graphite Negative Electrodes.* S.E. Trask, K.Z. Pupek, J.A. Gilbert, M. Klett, B.J. Polzin, A.N. Jansen, and D.P. Abraham, Journal of The Electrochemical Society, 163 (3) A345-A350 (2016).

1. Research Facilities Support

CAMP Facility Support Activities

Steve Trask, Alison Dunlop, Yimin Wu, Linghong Zhang, Gerald Jeka, Andrew Jansen, Bryant Polzin (Argonne National Laboratory)

Background

The Cell Analysis, Modeling and Prototyping (CAMP) Facility at Argonne National Laboratory is providing support to this project in a number of different ways. The main contributions to the project are: providing standard materials, providing baseline electrodes (both anodes and cathodes) that are capacity matched, providing experimental electrodes are needed, and providing electrochemical data from coin cells and pouch cells that were tested by the CAMP Facility. By having access to these materials, electrodes and data, other participating laboratories in the project are able to characterize the same materials using different techniques and test these materials in different configurations and are able to compare data across all laboratories working in this project. This provides a greater knowledge data pool for this project to draw from.

Results

In this Quarter we worked on three main tasks, produced new silicon/graphite electrodes, identified and distributed a new baseline silicon/silicon oxide powder, and physically characterized the new baseline silicon/silicon oxide powder.

Three new electrodes were added to the CAMP Facility's Electrode Library for this project. The first electrode is an anode with a composition of: 73 wt% Hitachi MAGE3 graphite, 15 wt% Paraclete Energy Si/SiO (150nm) powder, 2 wt% Timcal C45 Carbon Black and 10 wt% LiPAA. This electrode was labeled A-A012 and had a total electrode loading of 3.63 mg/cm². When half coin cells were tested with this electrode, an area capacity of ~2.31 mAh/cm² (at 1C) was achieved. When matched against the NMC532 cathode for this project, the n:p ratio was higher than acceptable. For this reason, a second electrode with the exact same composition as above was re-produced. In this case, the electrode ID is A-A013 and it has a total electrode loading of 3.00 mg/cm². When half coin cells were tested with this electrode, an area capacity of 1.91 mAh/cm² (at 1C) was achieved which gives an n:p ratio of ~1.1-1.2 against the NMC532 cathode electrode used in this project. The last electrode that was produced was a plain graphite electrode. In the last year we have moved from the Hitachi MAGE graphite that we use in our blended electrodes to the newer Hitachi MAGE3 graphite. The electrode composition that was produced was: 91.83 wt % Hitachi MAGE3, 2 wt% Timcal C45 carbon black, 6 wt% Kureha 9300 PVDF binder and 0.17 wt% Oxalic Acid. This electrode is meant to be a baseline electrode of just graphite. The electrode ID for this electrode is A-A016.

The second task that was completed in Q1 was the identification of a new baseline silicon/silicon oxide powder. Argonne National Laboratory has been working with Paraclete Energy (Chelsea, MI), which is a domestic producer and supplier of various silicon products for lithium ion battery applications. Paraclete Energy has been selected as a supplier of a non-surface-modified silicon metal particle with a silicon oxide coating and a particle size of ~150 nm for the consortium. By working with Paraclete Energy, the consortium has a source of material where the process for producing the material is known and can be reproduced over

multiple batches. Having this process knowledge and consistent material provides a good baseline material to evaluate the performance of the nano-silicon particles in lithium-ion battery applications. Early in Q1, 4 kilograms of the non-surface-modified silicon metal particle with a silicon oxide coating was ordered and delivered by Paraclete Energy. Since then, ~2 kgs of this material was distributed to the various labs participating in this project.

The last task that was completed in Q1 was the physical characterization of the 4 kg batch of non-surface-modified silicon metal particle with a silicon oxide coating powder. The Lot ID for this material is F17-021-LS. The same methods of characterization were used to evaluate this batch of material as past materials: Particle Size Distribution, SEM images, TGA, and NMR.

The first characterization that was done on the material was particle size analysis. The results from the testing show a D10 of 0.02 microns, D50 of 0.11 microns, D90 of 0.31 microns. The shape of the particle size distribution curve is a nice bell curve with a mean particle diameter of 0.15 microns.

The next characterization that was done was to examine the particle morphology using the SEM. From the image we can see that the particles are smooth and have a nice semi-rounded shape.

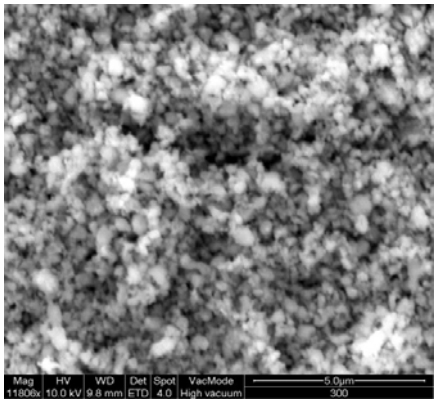

Figure 1. SEM Image of Paraclete Energy Silicon Powder (Lot # F17-021-LS)

The next characterization that was done was to examine the material was Thermo Gravimetric Analysis. In this analysis we are looking for any leftover solvent or unreacted silicon metal that did not oxidize during heat treating. From this testing, a 1.3 wt% gain was achieved, which is what would be expected when heating up to 1000°C. This shows that there is no leftover solvents and that the surface of the particles are well reacted with oxygen.

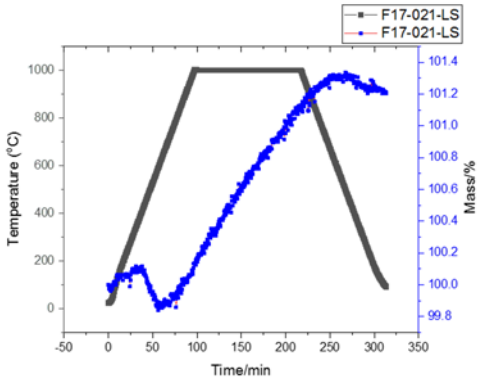

Figure 2. TGA Analysis of Paraclete Energy Silicon Powder (Lot # F17-021-LS)

The last materials characterization that was done was to examine quality via NMR analysis. This testing is currently ongoing and will be reported when it is completed.

Conclusions

As in past quarters, the CAMP Facility continues to provide the materials and data necessary to the project so that the overall project can move forward with consistent results. The CAMP Facility will continue to provide material support to this project in future quarters and will present new data as it comes available.

Proposed Mechanism for the Gassing of Si in Water Slurries

Kevin Hays (Oak Ridge National Laboratory), Baris Key (Argonne National Laboratory), Gabriel Veith (Oak Ridge National Laboratory)

Background

Recent studies have observed H_2 gas formation during larger scale preparation (> 1 L) in water based Si slurries, resulting in the oxidation of the Si particles.[1] The occurrence of H_2 poses safety concerns, as current production methods involve mixing slurries in large sealed planetary mixers, allowing for pressurization of this flammable gas. To date there has been no studies to understand what is occurring in this oxidation, the rate and mechanism of reaction, how silicon based chemistry affects the reaction, and how this controls performance.

Results

Slurries comprised of Si powder (Nanoamor, 70-130 nm [NA 70-130] or Alfa Aesar, 325 mesh [AA 325]) carbon black (CB, Imerys, C45) and 1.3 g of LiPAA in water or NMP were prepared in a sealed high pressure vessel. A summary of results can be found in Table 1. In all mixtures gas production/consumption reactions were measured though the extent of reaction varied significantly depending on the reagents. The slurry mixtures that produced H_2 gas include W2, W4, and W5. W2 and W4 both used NA 70-130 and both contained CB. Based on this observation, it seems more likely that the action of mixing the CB with Si, to attain intimate contact between these particles, appears to be the more crucial component to moving this H_2 producing reaction forward. We believe the CB acts as a high surface area catalytic site in which a proton coupled, charge transfer could take place,[2] following the scheme found in Figure 1left. Both OH^- and H^+ readily diffuse through amorphous SiO_x.[3] Despite the acidic environment, the natural dissociation of water provides sufficient OH^- ions, which could diffuse through the amorphous SiO_x and oxidize the Si^0 core according to the equation:

$$Si(s) + 2\ OH^-(aq) \rightarrow SiO_2(s) + 2\ H^+(aq) + 4\ e^-$$

This is followed by the reverse diffusion of H+ opposed to molecular H_2, which alleviates the need for additional porosity to allow the escape of gas. The diffusion of 2 H^+ out of the SiO_x occurs in tandem with a 4 e^- transfer to the local CB, providing a site for aqueous H+ reduction, eqquation:

$$2\ H^+(aq.) + 4\ e^- \rightarrow 2\ H_2(g).$$

In this proposed scenario the CB lowers the activation energy needed to reduce the protons, which may not take place on the SiO_x surface alone.

Table-1: Summary of Slurry Samples and selected results

Sample ID	Si particle	CB	Binder	Solvent	Slurry pH	Δ Oxide Thickness (nm)	Δ P 100 h (atm)	Δ P 20 h (atm)	H_2 produced	O_2 consumed
W1	NA 70-130	No	No	water	5.7	5	-0.01	0	No	Yes
N1	NA 70-130	Yes	No	NMP	N/A	4.5	-0.03	-0.01	No	Yes
W2	NA 70-130	Yes	No	water	5.3	7.5	0.22	0.04	Yes	Yes
W3	NA 70-130	No	Yes	water	6.3	5	-0.01	-0.01	No	Yes
W4	NA 70-130	Yes	Yes	water	6.8	7.5	0.47	0	Yes	Yes
W5	AA 325	No	No	water	-	2	1.27	0.16	Yes	Yes

Knowing that processing Si in water, under certain conditions, causes a change in the oxide content and surface chemistry, we cycled Si based half cells with and without the 100 hours of mixing. Unprocessed, or short time mixing NA 70 – 130 Si was compared to W2 to identify differences in electrochemical performance. In the voltage profile, shown in Figure 1(right), the half cell containing the unprocessed Si has a 1st cycle unload capacity of 1392 mAh g^{-1}. The 2nd cycle unload capacity decreases to 1128 mAh g^{-1}. The half cell containing W2 has 1st and 2nd unload capacities of 566.9 and 417.4 mAh g^{-1}, respectively. While this slurry formulation was not optimized, accounting for the lower than theoretical capacity, it is immediately noticeable that the 1st cycle unload capacity is of the unprocessed Si is more than twice the capacity of W2. This could arise due to some portion of the Si particle becoming electrochemically inactive, due to a thick oxide shell, or because whole particles are electronically isolated because of poor mixing. The first circumstance seems more likely, because W2 was mixed for 100 h, compared to the unprocessed sample which was only mixed for a few minutes. Moreover, there is a larger hysteresis between the load and unload curves of the half cell containing W2. This also supports a thicker oxide shell on the Si particles that would decrease its electronic conductivity, leading to a larger IR drop. In addition to capacity, the 1st cycle coulombic efficiency of the half cell using the unprocessed Si is 64%, whereas W2 is 40%. This difference may result from the additional SiO_x in W2, which undergoes an electrochemical conversion to Li_2O, Li_2SiO_3, and Li_4SiO_4, or by the decomposition of more organic electrolyte.[4] Overall the half cell containing W2 only lost 149.5 mAh g^{-1} between the 1st and 2nd unload, where the unprocessed Si lost 264.1 mAh g^{-1}. This improved capacity retention between the 1st and 2nd cycle could result from better dispersion of W2 or because there was less electrochemically active Si overall in this electrode.

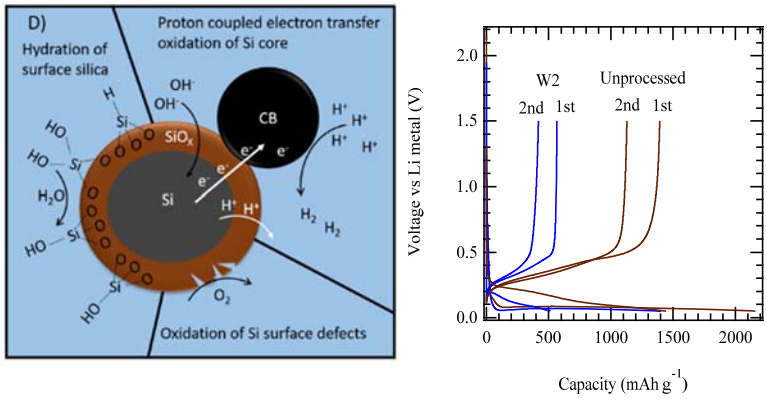

Figure 1 (left) Schematic of reactions occurring during processing; (right) capacity for the first two cycles of electrodes using short processing time or 100 hours in solution.

Conclusions

These results clearly indicate that the mixing process influences the materials chemistry AND capacity. This indicates some of the large variability in cycling performance could come from differences in processing times and conditions. These issues will be explored further in the future. Further details will be available in a full paper, which will be submitted by the end of the month.

References

1. Zhang, L.; Liu, Y.; Key, B.; Trask, S. E.; Yang, Z.; Lu, W., Silicon Nanoparticles: Stability in Aqueous Slurries and the Optimization of the Oxide Layer Thickness for Optimal Electrochemical Performance. *ACS Appl. Mater. Interfaces* **2017**.

2. Cabaniss, G. E.; Diamantis, A. A.; Murphy, W. R.; Linton, R. W.; Meyer, T. J., ELECTROCATALYSIS OF PROTON-COUPLED ELECTRON-TRANSFER REACTIONS AT GLASSY-CARBON ELECTRODES. *J. Am. Chem. Soc.* **1985,** *107* (7), 1845-1853.

3. (a) Hofstein, S. R., PROTON AND SODIUM TRANSPORT IN SIO2 FILMS. *IEEE Trans. Electron Devices* **1967,** *ED14* (11), 749-+; (b) Seidel, H.; Csepregi, L.; Heuberger, A.; Baumgärtel, H., Anisotropic Etching of Crystalline Silicon in Alkaline Solutions: I . Orientation Dependence and Behavior of Passivation Layers. *J. Electrochem. Soc.* **1990,** *137* (11), 3612-3626.

4. Philippe, B.; Dedryvere, R.; Allouche, J.; Lindgren, F.; Gorgoi, M.; Rensmo, H.; Gonbeau, D.; Edstrom, K., Nanosilicon Electrodes for Lithium-Ion Batteries: Interfacial Mechanisms Studied by Hard and Soft X-ray Photoelectron Spectroscopy. *Chem. Mat.* **2012,** *24* (6), 1107-1115.

Thermodynamic Understanding and Abuse Performance

Kyle Fenton, Eric Allcorn, and Ganesan Nagasubramanian (Sandia National Laboratories)

Background

As we develop new materials to increase performance of lithium ion batteries for electric vehicles, the impact of potential safety and reliability issues become increasingly important. In addition to electrochemical performance increases (capacity, energy, cycle life, etc.), there are a variety of materials advancements that can be made to improve lithium-ion battery safety. Issues including energetic thermal runaway, electrolyte decomposition and flammability, anode SEI stability, and cell-level abuse tolerance behavior. Introduction of a next generation materials, such as silicon based anode, requires a full understanding of the abuse response and degradation mechanisms for these anodes. This work aims to understand the breakdown of these materials during abuse conditions in order to develop an inherently safe power source for our next generation electric vehicles.

The effect of materials level changes (electrolytes, additives, silicon particle size, silicon loading, etc.) to cell level abuse response and runaway reactions will be determined using several techniques. Experimentation will start with base material evaluations in coin cells and overall runaway energy will be evaluated using techniques such as differential scanning calorimetry (DSC), thermogravimetric analysis (TGA), and accelerating rate calorimetry (ARC). The goal is to understand the effect of materials parameters on the runaway reactions, which can then be correlated to the response seen on larger cells (18650). Experiments conducted showed that there was significant response from these electrodes. Efforts to minimize risk during testing were taken by development of a smaller capacity cylindrical design in order to quantify materials decision and how they manifest during abuse response.

In order to try and quantify these effect, 18650 cells were made with electrodes cut to a much smaller overall cell capacity of roughly 600 mAh nominal capacity. The excess space within the cell was minimized using a copper insert to keep the ratio of electrolyte to electrode material constant. The comparison between graphite anodes and those containing up to 15% silicon can be seen in Figure 1.

Results

This work continues the efforts from last year, which aim to understand the fundamental reactions and quantify response from silicon based anodes under abusive conditions. This included evaluation of anodes containing between 0 and 15 wt% silicon from a variety of sources. Investigations were completed on coin cell and 1.25 Ah 18650 form factors. Several experiments showed a high level of gas generation and overall runaway for cells containing silicon electrodes. To further understand the response of these materials, this work focused on understanding the effect of several factors impacting runaway response and gas generation including solvent selection, electrode processing, silicon content, and the effect of water. Previous efforts to evaluate these parameters in 18650 cell form factors using accelerating rate calorimetry (ARC) proved difficult due to the gas generation and temperatures involved during runaway.

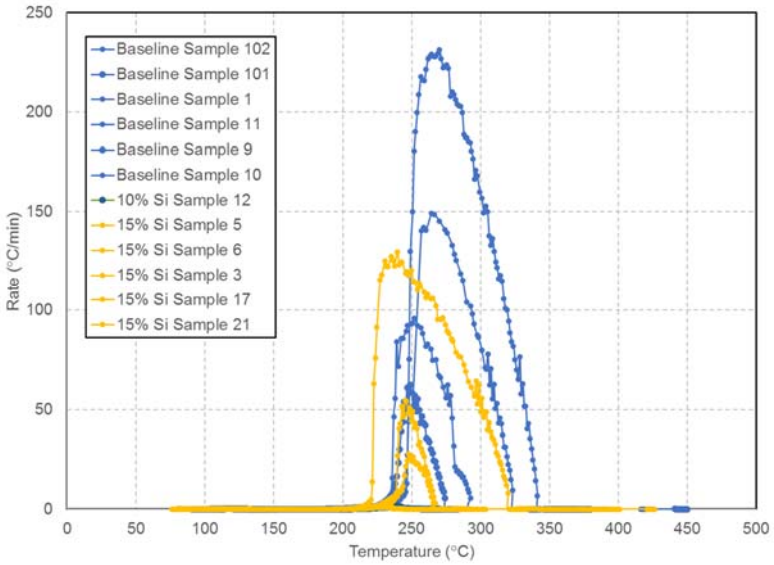

Figure 1 - Accelerating rate calorimetry (ARC) response for 18650 cells with graphite anodes (blue), 10 wt% silicon (green), and 15 wt% silicon (yellow). Heating rate is not normalized to active material content, so peak heating rates and overall runaway enthalpy is shown for qualitative purposes only.

Figure 1 shows ARC response for 18650 cells with graphite anodes (blue), 10 wt% silicon (green), and 15 wt% silicon (yellow). Heating rate is not normalized to active material content, so peak heating rates and overall runaway enthalpy is shown for qualitative purposes only. The overall response of the cells are very similar between graphite and silicon based composite electrodes. This result contradicts many of the observations seen in previous evaluation of silicon anode materials. Gas samples were taken during testing and analyzed to evaluate species evolved during runaway. Gas analysis showed that the silicon containing electrodes generated higher levels of short chain hydrocarbons (ethane and propane), had less short chain organics (ethanol and propene), and similar concentrations of carbon dioxide and carbon monoxide. The overall gas generated in silicon based cells was about twice that generated in graphite containing cells.

In an effort to fully understand silicon contribution to abuse response, electrodes were made with newly acquired Paraclete Energy 100 nm silicon materials. Silicon, Hitachi Mag-E graphite, Timcal C45 carbon, and lithium polyacrylic acid (LiPAA) were used in weight percentage ratios of 15/73/2/10 respectively. Electrodes parameters were 55 µm thickness, 45 % porosity, and areal capacity of 3.3 mAh/cm^-2. This was then coated and put on formation cycling in half cell configuration as seen in Figure 2. Overall, this material exhibits a high first cycle coulombic efficiency of 89 % and stable cycling for the first 5 cycles at approximately 600 mAh/g. Evaluations are ongoing to evaluate the response of this material to abuse conditions and understand the mechanisms observed during runaway.

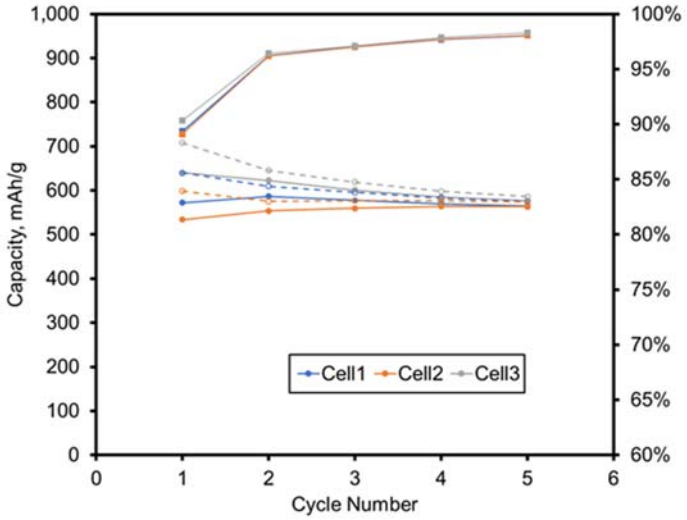

Figure 2 - Half cell electrochemical cycling performance of 15% Paraclete nSi anodes cycled at C/10 from 1.5V – 0.05V vs. metallic lithium.

Conclusions

This work demonstrates that there is an impact on safety response with nanoscale silicon materials compared to graphite based anodes. Changes to material and cell level properties can have impact on safety and thermal response characteristics. We have reported thermal runaway properties of cells (coin cells and cylindrical cells) containing nanoscale silicon up to 15 percent by weight. We continue to develop the understanding of abuse response for these anodes to better understand how these next generation negative electrode materials will impact cell and battery-level abuse tolerance. Additionally, the fundamental reactivity and gassing behavior that has been observed in silicon offers opportunities for better understand the safety of these materials.

2. Characterization, Diagnostics, and Analysis

Electrode heterogeneity after processing

Rose Ruther (Oak Ridge National Laboratory)

Background

We have been using Raman spectroscopy as a tool to characterize heterogeneity in silicon-graphite composite electrodes. Our results clearly show evidence for phase segregation and non-uniform electrochemical cycling of silicon. This indicates that the processing science for forming composite electrodes with disparate materials needs to be better understood. Electrode heterogeneity and non-uniform lithiation is a primary driver of battery failure.

Results

Single-layer pouch cells were built at the ORNL BMF with silicon-graphite composite anodes (A-A006A) and $LiNi_{0.5}Mn_{0.3}Co_{0.2}O_2$ cathodes (A-C013A) coated by the CAMP facility at ANL. Cells were cycled using the standard electrolyte and cycling protocols. Anodes were analyzed by Raman spectroscopy without air exposure. To visualize anode heterogeneity, Raman maps were analyzed using a combination of cluster and basis analysis.

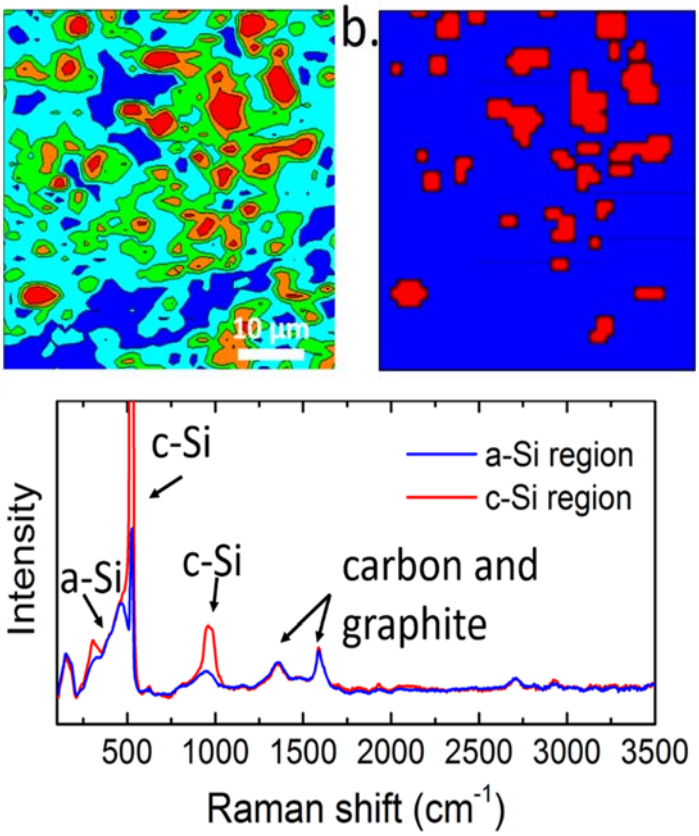

Figure 1. (a) Raman map of the intensity of the main band from crystalline silicon at 520 cm^{-1} in a silicon-graphite composite electrode after 1 charge-discharge cycle. The fraction of crystalline silicon increases from blue to red. (b) Two level map of the same data presented in (a). The red pixels are from the electrode areas with the highest concentration of crystalline silicon. (c) Average Raman spectra from regions with high and low concentrations of crystalline silicon mapped in (b).

We observed domains of crystalline Si in cycled composite anodes (Figure 1a). This indicates that some fraction of the Si is electrochemically inactive, does not lithiate, and does not undergo the transition to amorphous Si. Inactive Si was observed even after 100 cycles in full cells and in half cells with a virtually infinite supply of active lithium. To understand if the inactive regions of the electrode could be electronically isolated, we binned the Raman spectra from a map over a large area (50 x 50 µm, 2500 pixels) into two groups to separate out the spectra with the largest fraction of crystalline silicon (Figure 1b). No difference in the intensity of the bands from carbon and graphite were observed in the spectra with the most crystalline silicon compared to all other regions of the electrode (Figure 1c). Differences in carbon content do not explain why some Si is electrochemically inactive and suggest that electronic conductivity is not the limiting factor. Ongoing work will evaluate how improvements in electrode processing (control over surface charge, order of mixing, and binder chemistry) impact electrode homogeneity. Uniform lithiation is critical to improve active material utilization and increase battery lifetime.

EQCM Studies of Silicon Anodes

J. Vaughey, Niya Sa, Binghong Han (Argonne National Laboratory)

Background

The DeepDive silicon program seeks to develop an understanding of the failure mechanisms of a silicon-based LIB anode and how the properties of a silicon-based electrode lead to those instabilities and short cell lifetimes. Many of the instabilities are thought to arise from the silicon particles SEI layer – its formulation, constituents, and dimensional stability – that acts as a buffer between the electrolyte and electrode surface. As the primary protective layer in a lithium-ion energy storage system, understanding the SEI layer is critical to defining and understanding various failure mechanisms that lead to performance degradation as many of the causes of capacity fade and poor coulombic efficiency are, at their core, derived from an unstable SEI layer [1-4]. The reactivity of the surface of the silicon electrode is key to understanding the growth and stability of the SEI layer. In the DeepDive program we are focused on evaluating Si thin films during cycling to assess their reactivity with electrolytes using EQCM spectroscopy. This project addresses the stability of the electrode and

the associated problems of the reactivity of the active material towards the constituents of the cell. This buildup of reaction products contributes to the fundamental problem of cycle to cycle instability associated with SEI layer.

Results

Efforts in the DeepDive program are focused on the synthesis and evaluation of thin film electrodes and their reactivity with the electrolyte. These surface based reactions are an important source of electrons and the formed organic reaction products that become substituents for the silicon SEI layer. Our thin film effort has been distributed over two parts. We participated in the round robin thin film effort organized by Gabe Veith (ORNL) to assess the ability to baseline Si film electrodes. In these round robin efforts, we submitted ANL-created Si films to the program and evaluated common films created at ORNL. The capability to make PVD Si films for the program at Argonne is derived from the need to have Si-coated sensors for our EQCM studies. In the initial studies, the ANL created films were evaluated versus the other labs and found to exhibit higher capacity than anticipated rom the amount of silicon deposited. The majority of the extra capacity was found to occur at a potential of approximately ~1.2V (vs Li). ORNL was able to show that offsetting the 1st cycle data made a good approximation to the other labs results, indicating the reaction to produce the extra capacity may be exterior to the active silicon particles. Looking at the history of the samples studied indicated that either the films were contaminated in the PVD chamber (Bi target in chamber) or the copper foils were partly oxidized by the process. Literature analysis and further XPS studies led us to believe that the most likely impurity were phases on the underlying copper foil (i.e. Cu_2O). Literature values had indicated Cu_2O decomposes around 1.3V (vs Li) while Bi lithiates (to Li_3Bi) around 1V. Subsequent round robin studies did not show this extra capacity and data fell in line with the other test centers.

Continued EQCM studies of the films (thin film CV; Figure 1) indicate a break-in process that is tied to more increased mass deposited on the surface of the electrode with an increase in the porosity of the SEI layer formed. SEM studies indicate film cracking (higher surface area) and issues associated with delamination of the film from the EQCM sensor have been occurring. The film underlayer (Au vs Cu) has been initially as a contributing cause of the delamination; copper was identified as being the better choice due to side reactions with Au (formation of Li_2Au).

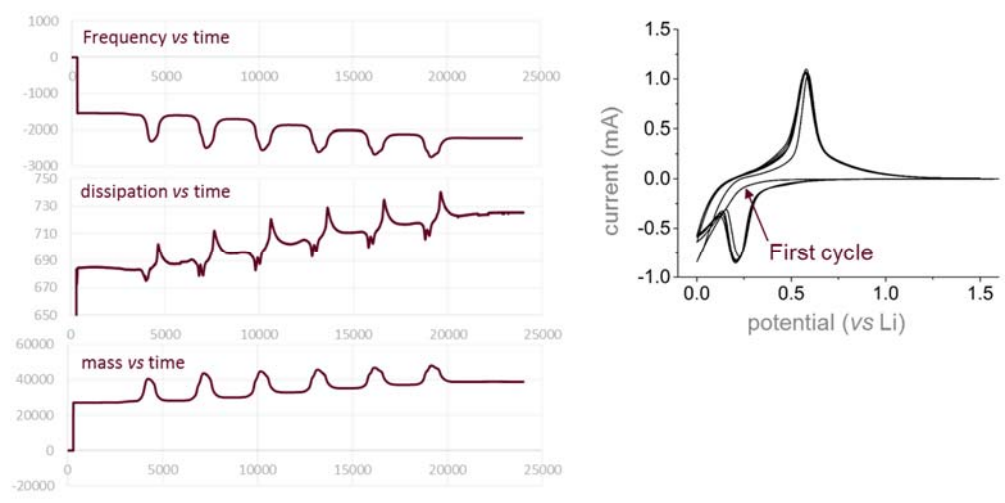

Figure 1. *CV is scanned from the OCV (~2.8 V vs Li) to 0.001 V at 1 mV/sec. Si is cycled at least for 5 cycles to collect electrochemical information, frequency change and the dissipation is monitored simultaneously*

Conclusions

The SEI layer of silicon is a complex, every changing component of the lithium-based electrochemical cell. Our effort within the program is concerned with developing an understanding of how the silicon (Li_xSi, Li_xSiO_y) species within the electrode interacts with their environment to produce the components observed within the SEI layer. We have synthesized and scaled up single phase compounds that represent the silicon electrode at various states of charge and using MAS-NMR, EQCM, Raman, and X-ray diffraction started assessing the types of phases formed at the electrode-electrolyte interface as a function of state of charge.

References

[1] Alison L. Michan, G. Divitini, A. J. Pell, M. Leskes, C. Ducati, Clare P. Grey *J. Am. Chem. Soc*., **138**, 7918−7931 (2016)
[2] Sung-Yup Kim, Yue Qi *J. Electrochem. Soc*, **161**, F3137-F3143 (2014).
[3] Bertrand Philippe, R. Dedryvère, M. Gorgoi, H. Rensmo, Danielle Gonbeau, Kristina Edström *Chem. Mater*., **25**, 394−404 (2013).
[4] Aude A. Hubaud, Z.Z. Yang, D. J. Schroeder, Fulya Dogan, L. Trahey, J. T. Vaughey *J. Power Sources* **282**, 639-644 (2015).
[5] C. J. Wen, R. Huggins *J. Solid State Chemistry*, **37**, 271-278 (1981).

Synthesis and electrochemical performance of Li_2SiO_3-coated silicon nanoparticles

Linghong Zhang, Kaushik Kalaga, Daniel Abraham, Wenquan Lu (Argonne National Laboratory)

Background

Silicon is a promising anode material for lithium-ion batteries due to its high gravimetric and volumetric capacities. However, it suffers from substantial capacity fade over cycles due to its ~300% volumetric change during lithiation/delithiation. The dramatic volumetric change leads to pulverization and fracture of the particles as well as exposure of new surfaces to the electrolyte, resulting in accelerated parasitic reactions. In order to improve its capacity retention, methods to improve the mechanical stability of Si particles need to be investigated.

A Li_2SiO_3 coating has been reported beneficial for Li-ion batteries. When such a coating is present for a $LiNi_{0.6}Co_{0.}2Mn_{0.2}O_2$ cathode, improvement in both rate and cycle performance is observed owing to the excellent ionic conductivity of Li_2SiO_3 as well as the enhanced structural stability it provides.[1] A coating containing Li_2SiO_3 has also been applied to the Si anode. The resulting material showed improved capacity retention, however, with a compromised specific capacity.[2] Nonetheless, the improved capacity retention suggests that the Li_2SiO_3 coating may also improve the mechanical stability of the Si nanoparticles.

In order to further evaluate the effect of a Li_2SiO_3 coating on the electrochemical performance of Si nanoparticles, Li_2SiO_3-coated silicon nanoparticles were synthesized via solid-state reaction. The particles were then characterized and tested for electrochemical performance.

Results

Figure1 shows the diagram for the synthesis of silicate-coated silicon nanoparticles. In order to obtain Li_2SiO_3-coated silicon nanoparticles, the Si nanoparticles with an average diameter of 80 nm were first treated at 400℃ in the air for 15 hours to obtain a surface oxide layer with a proximate thickness of 3 nm. The 400℃-treated Si nanoparticles were then mixed with Li_2CO_3 with a molar ratio of n(Si in SiO_2): n(Li in Li_2CO_3) = 1:2, and heat-treated at 800℃ under Ar atmosphere for 6 hours before collection for characterization.

Figure 1 Diagram for the synthesis of Li_2SiO_3-coated silicon nanoparticles

Figure 2 shows the scanning electron microscopy (SEM) images for the pristine Si nanoparticles as well as the particles after the solid-state reaction with Li_2CO_3. The pristine Si nanoparticles in Figure 2a are spherical with the particle size ranging from approximately 50 nm to 300 nm. The heat treatment in air at 400°C did not result in a change in particle size and morphology, as has been confirmed by transmission electron microscopy previously, suggesting minimal sintering at 400°C. Figure 2b shows the Si nanoparticles after the solid-state reaction with Li_2CO_3. While the size of the primary particles is still comparable to the pristine Si nanoparticles, the particles appear to be interconnected with each other, forming larger aggregates.

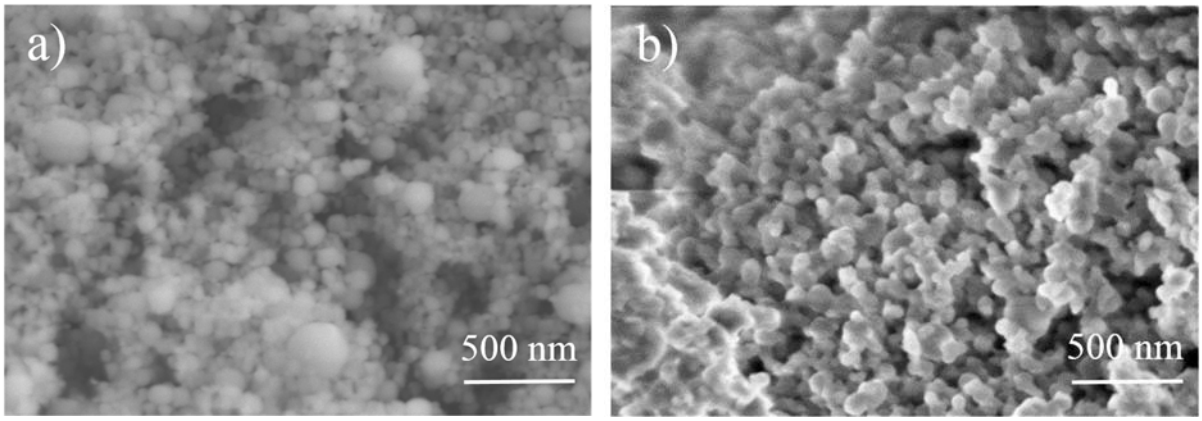

Figure 2 SEM images of a) pristine Si nanoparticles, and b) Li_2SiO_3-coated Si nanoparticles

The silicate-coated Si nanoparticles were then characterized by x-ray diffraction. Figure 3 shows the x-ray diffraction pattern of the Li_2SiO_3-coated Si nanoparticles. The spectrum revealed the presence of crystalline Si as well as crystalline Li_2SiO_3 phase, confirming the formation of Li_2SiO_3 shell outside a Si core.

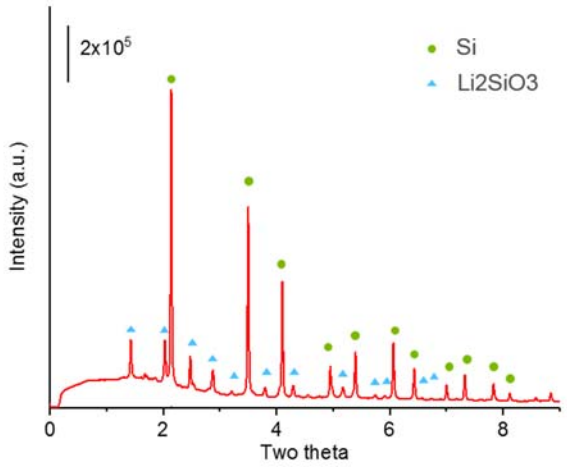

Figure 3 X-ray diffraction pattern of Li_2SiO_3-coated Si nanoparticles

The Li_2SiO_3-coated Si nanoparticles were then fabricated into laminates with 20 wt% LiPAA and 10 wt% C45. The electrodes were then tested in half-cell configuration with Gen II electrolyte (EC: EMC=3:7) with 10 wt% FEC. The cells first underwent three formation cycles at C/10 rate between 1.5 V and 0.01 V. Figure 4 compares the electrochemical performance of formation cycles for pristine Si nanoparticles, 400°C-treated Si nanoparticles, and Li_2SiO_3-coated Si nanoparticles. Compared with pristine and 400°C-treated Si nanoparticles, Li_2SiO_3-coated Si nanoparticles showed a decreased specific capacity and a slightly improved coulombic efficiency. A decrease of capacity to ~2250 mAh/g is expected for the silicate-coated Si nanoparticles as a silicate layer takes up a larger weight fraction compared to an oxide layer. However, a low specific capacity of 1900 mAh/g suggests the presence of other factors. For example, if the Li_2SiO_3-coated Si nanoparticles present in the electrode as aggregates, the impedance of the cell can increase and fully lithiation of the electrode can be more difficult. The Li_2SiO_3-coated Si nanoparticles were also used without further washing to remove possible residues. The presence of residues from the solid-state reaction may also result in the low specific capacity. Future work is needed to test the long-term cycle performance of silicate-coated silicon, to investigate the cause of the low specific capacity as well as to optimize the electrode formulation and silicate thickness to optimize the electrochemical performance.

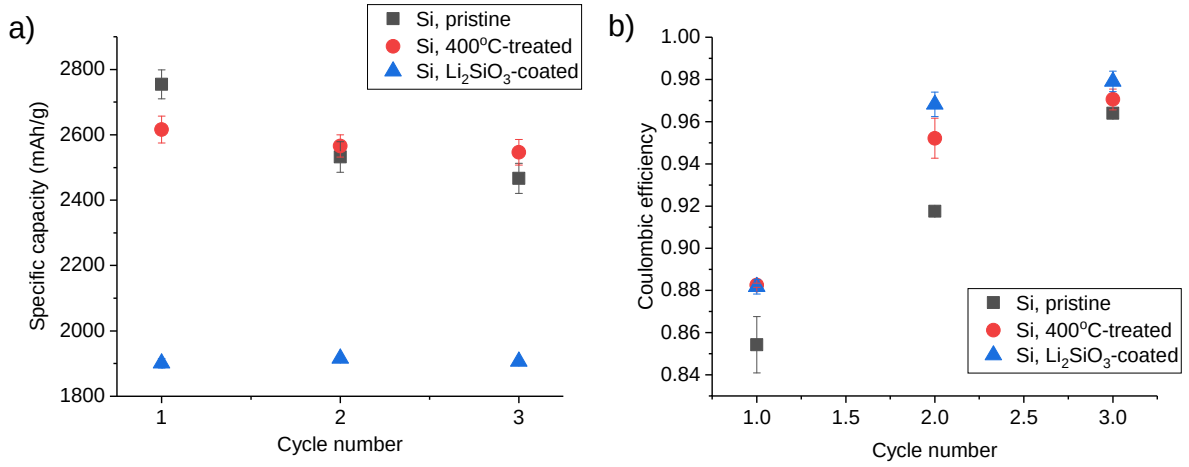

Figure 4 Electrochemical performance of formation cycles for pristine Si nanoparticles, 400°C-treated Si nanoparticles, and Li_2SiO_3-coated Si nanoparticles.

Conclusions

Li_2SiO_3-coated Si nanoparticles were successfully synthesized via solid-state reaction with Li_2CO_3. The electrochemical performance of Li_2SiO_3-coated Si nanoparticles showed a low specific capacity and a slightly improved coulombic efficiency in the formation cycles. The low specific capacity could result from the increased impedance due to the presence of aggregates in the electrode. Future work should include: 1. Investigate the reasons for the low specific capacity in the formation cycles and improve it, 2. Study the effect of silicate coating thickness on the electrochemical performance of Si nanoparticles, and 3. Study the effect of other silicate coatings such as a Li_4SiO_4 coating.

References

1. Wang *et al*. "Enhanced electrochemical performance of lithium metasilicate-coated LiNiCoMnO2 Ni-rich cathode for Li-ion batteries at high cutoff voltage", Electrochimica Acta, 2016, **222**, 806-819
2. Lee *et al*. "High-performance silicon-based multicomponent battery anodes produced via synergistic coupling of multifunctional coating layers", Energy Environ. Sci., 2015, **8**, 2075-2084

Calendar-life versus Cycle-life aging of Lithium-ion Cells with Silicon-Graphite Composite Electrodes – Electrochemistry Data

K. Kalaga, M.-T.F. Rodrigues, S.E. Trask, I.A. Shkrob, D.P. Abraham (Argonne National Laboratory)

Background

The use of blended silicon-graphite (Si-Gr) negative electrodes increases the energy density of lithium-ion cells over those containing only graphite (Gr) electrodes. However, volume changes in the Si particles that occur during cycling causes deterioration of the solid-electrolyte interphase (SEI) layer on the particles resulting in further electrolyte reduction that immobilizes Li^+ ions and, therefore, capacity fade. A natural question to ask is whether the observed fast capacity fade in Si-Gr electrodes vs. Gr electrodes (for which the volume variation is < 10%) is solely due to the volume changes, or if there are other compounding factors that are specific to Si particles alone? To answer this question we developed a calendar-aging test, which included a potentiostatic hold. Cells with Si-Gr and Gr negative electrodes (and $Li_{1.03}(Ni_{0.5}Co_{0.2}Mn_{0.3})_{0.97}O_2$ containing positive electrodes) were assembled, tested, and compared using complementary cycle-life and calendar-life aging protocols. Because the Si particles volume changes are not expected to occur during a potentiostatic hold, by comparison of data from the cycle-life and calendar-life aging tests we were able to assess the role of volume changes in the deterioration of cell cycling performance.

Results

Potential profiles for the positive electrode from a NCM523/Si-Gr (10 wt% FEC) cell that underwent cycle-life aging is shown in Fig. 1a and from a similar cell that underwent calendar-life aging is shown in Fig. 1b. The negative electrode potential is simply the difference between the cell voltage and positive potential at any given instant. For example, cycle 2 in Fig. 1a indicates that the positive potential changes from 3.68 V to 4.22 V (as a result of oxide delithiation), when the cell is charged from 3.0 to 4.1 V; the negative potential correspondingly changes from 0.68 V to 0.12 V (indicating lithiation of the Si-Gr electrode). The reverse process happens during cell discharge from 4.1 to 3.0 V; the positive potential changes from 4.22 V to 3.68 V (as a result of oxide lithiation), and the negative potential correspondingly changes from 0.12 V to 0.68 V (indicating delithiation of the Si-Gr electrode).

As the cell is cycled, the positive potentials at the end of charge and discharge gradually increase over the 100 cycles, and the cycling window narrows. For example, when the cell is charged from 3.0 to 4.1 V at cycle 99, the positive potential changes from 3.77 V to 4.29 V (Fig. 1a). The higher upper potential (4.29 V vs. 4.22 V at cycle 2) indicates increasing delithiation of the oxide during cycling and the narrower cycling window (0.52 V vs. 0.54 V at cycle 2) indicates ongoing capacity loss. The observed changes can be obtained by the electrode

potential shifts (known as "voltage slippage") that occur during cell cycling. This slippage, results from a net loss of mobile Li^+ ions, as they become incorporated into the solid electrode phase (SEI) of the Si-Gr negative electrode. The capacity loss (cycle 99-cycle 2, C/20 rate) for the cell is ~44 %.

For the calendar-life test cell, electrode potential changes during the formation cycles are similar to that of the cycle-life cell, as expected. During the potentiostatic hold the positive electrode potential of this cell also increases, indicating increasing delithiation of the oxide (Fig. 1b). However, after the potentiostatic hold, the positive potentials at the end of charge and discharge are *slightly lower* than those before the hold. For example, the highest potential for cycle 5 is 4.227 V vs. 4.233 V for cycle 3; the lowest potential for cycle 5 is 3.714 V vs. 3.716 V for cycle 3. The capacity change during the 600 h potentiostatic hold was obtained through measurements of small parasitic currents, flowing through the cell: in Fig. 1b, 11.1 mAh/g charge was transferred between the electrodes during the 600 h potentiostatic hold.

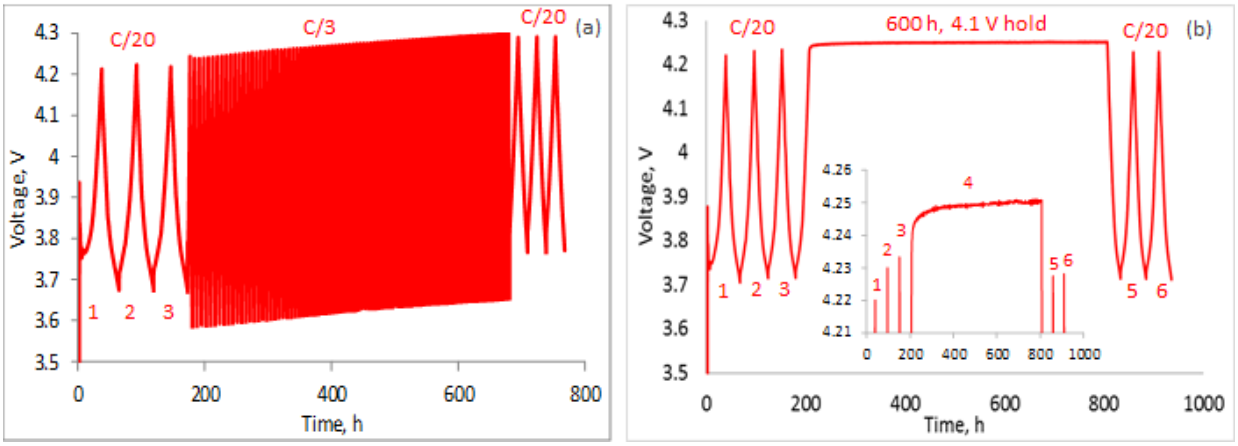

Figure 1. Changes in the positive electrode potential during (a) cycle-life aging and (b) calendar-life aging of a NCM523/Si-Gr (10 wt% FEC) cell. The inset in (b) shows the top 50 mV of the plot. In both plots, the first 3 (formation) cycles are at a ~C/20 rate. In (a), cycles 4-97 (aging) are at a ~C/3 rate and cycles 98-100 are at a C/20 rate. In (b), cycle 4 includes a 600 h hold after charging to 4.1 V; the cycle 4 discharge and the final diagnostic cycles 5 and 6, are at a C/20 rate.

A possible explanation for the observation in Fig. 1b is as follows: additional sites for Li^+ ion insertion in the negative electrode become available during the potentiostatic hold. These "higher impedance" sites, presumably in the silicon, are not accessible during typical charging, even at a C/20 rate. Lithiation of these "additional" sites lead to increased delithiation of the oxide resulting in a higher potential at the positive electrode. However, SEI formation would also be expected at these newer sites, leading to some irreversible loss of Li^+ ions. The measured capacity loss of cycle 4 (4.5 mAh/g) is the difference between the additional charge from accessing new sites and the charge consumed during SEI formation. The lower positive electrode potential during the fourth discharge results from the insertion of an additional charge into the oxide particles.

Conclusions

We compared the calendar-life and cycle aging behavior of several cells with a NCM523-based positive electrode and a Si-containing (or a Gr-based) negative electrode. The cells contained the baseline Gen2 electrolyte (1.2 M $LiPF_6$ in EC:EMC 3:7 w/w) with or without 10 wt% FEC. The conclusions from our data are as follows:

1. Capacity fade of the Si-containing cells was always greater than those of the Si-free cells, in both calendar and cycle-life tests.
2. Capacity fade was greater for the cycle-life tests than for the calendar life tests. The fade mainly results from immobilization of Li^+ ions in the negative electrode SEI.

3. A small parasitic current flow was observed in the cell during the potentiostatic hold; after ~100 h, the current flow was infrequent, indicating an SEI that is passivating for most of the time. However, periods of cell activity seen as random bursts of current flow indicate some charge loss to the SEI.
4. The Li^+ ion loss on our lithiated Si-Gr electrodes is small in the absence of volume changes. The repeated volume change of Si particles is indeed the leading cause for rapid capacity fade in Si-bearing cells.

3. Materials Advancements

High-Performance Polymer Binders for Silicon Anode in Lithium-ion Batteries

Peng-Fei Cao, Tomonori Saito (Oak Ridge National Laboratory)

Background

The development of Li-ion batteries with high energy density is highly necessary to fulfill the requirement of future electric vehicles for longer driving distance. Among the several anode materials with significantly high capacities, silicon is the most promising candidate to replace the currently used graphite due to its high theoretical gravimetric capacity (4212 mAh/g at high temperature and 3579 mAh/g at room temperature for silicon *vs* 372 mAh/g for graphite), low average voltage, and nature abundance. The severe capacity fade of silicon based electrode, which stemmed from the inherent volume expansion during alloying process (up to 280% for $Li_{15}Si_4$), occurs in several modes including pulverization of silicon anode, disconnection of active materials with conducting network and current collector, and instability of solid/electrolyte interface (SEI) layer. Although pulverization of the silicon anode can be resolved using nano-sized silicon materials, such as industrially scalable silicon nanoparticles (SiNPs, diameter ≤ 150 nm), binder material is still critical to maintain the electronic contact and stable SEI layers, and therefore enable stable cycle life for Si anode.

Several principles have been recognized as a design parameter for high-performance polymer binders: (1) adhesion capability with active material; (2) mechanical robustness; (3) forming a homogenous mixture (for active materials and conducting additive) with suitable solution viscosity.[1] Adhesion capacity of the polymer binders with the Si can contribute in two aspects: generate a protective layer on the surface of Si and suppress the decomposition of electrolyte; adhere the Si with the conducting additives and maintain the electronic contact of active materials. Mechanical robustness of polymer binders helps maintain the integrity of electrode morphology and minimize the destruction of electric pathways of active materials to their surrounding particles and current collectors. In-situ crosslinking to form a three dimensional network around the active material was demonstrated especially useful in preserving the integrity of silicon anode during cycling.[2] Forming a homogenous mixture and hence uniform anode coating on the current collector usually requires compatible chemical composition and optimized viscosity at required solution concentration range. Our recent work demonstrated significant architecture effect of polymer on binder performance in lithium-ion battery.[3] This project focuses on cultivating the fundamental understanding for the rational design of polymer binders for optimized Si binder performance using these principles.

Results

ORNL team has developed tailored functionalization on chitosan (CS-CG) and an efficient post cross-linking for the optimized performance. The significant viscosity increase and the shift of the IR spectra indicated successful crosslinking. Briefly, the crosslinker (GA) (e.g. 6 wt% to that of CS-CG) was added to the functionalized chitosan (CS-CG10%) to form a pre-crosslinked polymer solution (CS-CG10%+GA6%) which was mixed with silicon nanoparticles (SiNPs) and carbon black (CB). The SiNPs based composite film was dried at 80 ^oC under vacuum to remove extra moisture. Illustrated by the SEM image in Figure 1 (A), the obtained composite film exhibited porous architectures. Energy-dispersive X-ray spectroscopy (EDX) mapping of carbon and oxygen and especially silicon, which corresponding to the SiNPs, demonstrated the homogeneous distribution of active materials in the composite anode film. Optimized solution viscosity and functional groups of polymer binder solution should attribute to prevent aggregation of active materials during electrode fabrication process and contribute to the resulting homogenous dispersion.

PVDF and LiPAA (M_n=450,000) were utilized as the linear analogues for comparison purpose. As illustrated in Figure 2, a rapid capacity loss was observed for the silicon anode based on PVDF, and only less than 300 mAh/g capacity retained. The poor cyclability of the electrodes with PVDF binders indicates the isolation of SiNPs from the conduction network (or called "dead" silicon) after initial cycles. _ENREF_39Lack of interactions with silicon during the huge volume variation process may lead to the degradation of conduction network and isolation of SiNPs. LiPAA exhibited excellent cycling performance due to their enhanced adhesion interaction with the SiNPs based on anode.

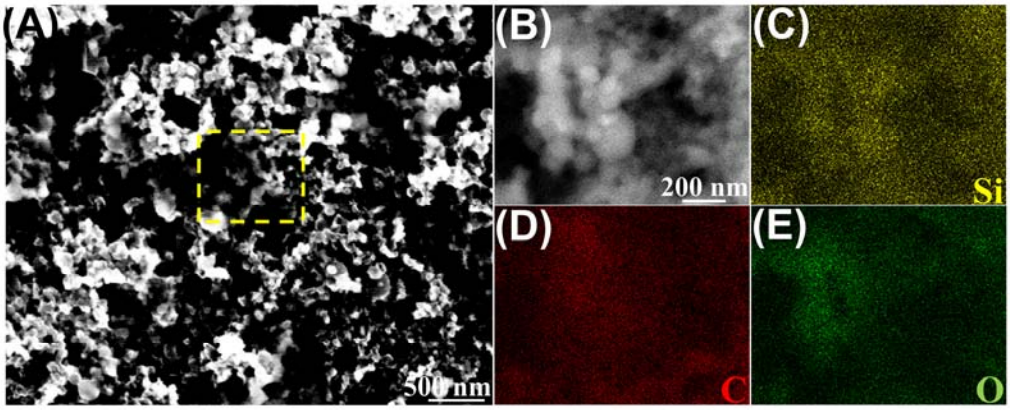

Figure 1. (A) SEM image of the SiNP based composite electrode with on copper foil,411608 (B), (C) Energy-dispersive X-ray spectroscopy (EDX) mapping and (D) Silicon distribution of the same electrode in A

CS also exhibited much better cycling performance than that of PVDF because the presence of hydroxyl and amine group may form physical interaction with SiNPs, which contribute to the stability of the conductive network around the SiNPs. After functionalization, improved cycling performance was obtained for the SiNPs based anode (CS-CG 10%) due the presence of adhesion capability. It can be seen from Figure 2 that the SiNPs anode with CS-CG10%+GA6% (optimized crosslinking ratio) as the binder exhibited significant improved cycling performance with retaining capacity of 2,200 mAh/g after 100 cycles.

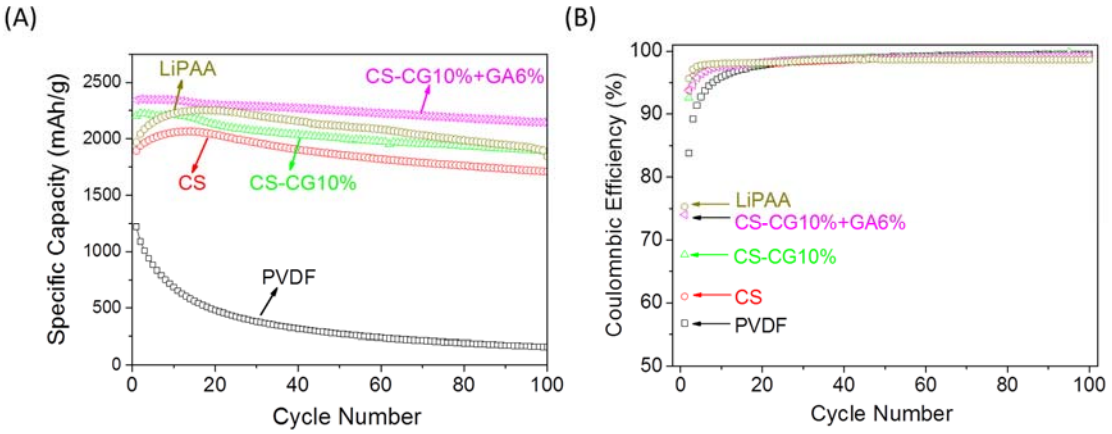

Figure 2. (A) Cycling performance silicon electrodes from the polymer binder of PVDF, CS, LiPAA, CS-CG10% and CS-CG10%+GA6% at a current rate of C/10; (B) Coulombic efficiency of the electrodes from different polymer binders.

Conclusions

A cross-linked functionalized chitosan (CS-CG+GA) network that possesses both adhesion capacity and mechanical robustness was demonstrated as the high-performance binder materials of Si electrode in lithium-ion battery applications. Our manuscript has been accepted to *ACS Applied Materials & Interfaces* (Ref 3) and our Invention Disclosure 201703938, DOE S-138,596, "Polymer Binder for Silicon/Graphite Anode in Lithium-Ion Batteries" was elected to pursue a patent application.

References

1. Choi, S.; Kwon, T.-w.; Coskun, A.; Choi, J. W., Highly elastic binders integrating polyrotaxanes for silicon microparticle anodes in lithium ion batteries. *Science* **2017,** *357* (6348), 279.
2. Gao, H.; Zhou, W.; Jang, J.-H.; Goodenough, J. B., Cross-Linked Chitosan as a Polymer Network Binder for an Antimony Anode in Sodium-Ion Batteries. *Advanced Energy Materials* **2016,** *6* (6), n/a-n/a.

3. Cao, P.-F.; Naguib, M.; Du, Z.; Stacy, E. W.; Li, B.; Hong, T.; Xing, K.; Voylov, D.; Li, J.; Wood, D. L.; Sokolov, A. P.; Nanda, J.; Saito, T., Effect of Binder Architecture on the Performance of Silicon/Graphite Composite Anodes for Lithium-ion Batteries. *ACS Applied Materials & Interfaces* **2018 ASAP**.

Lithiation Effect of the Poly(Acrylic Acid) Binders on the Silicon Anode of Lithium-Ion Batteries

Bin Hu, Sisi Jiang, Zhengcheng Zhang, and Lu Zhang (Argonne National Laboratory)

Background

Silicon (Si) stands out as a next-generation active anode material due to its high specific capacity of ~ 4200 mAh/g and high volumetric capacity of ~ 2400 mAh/cm^3 compared to graphite and also with some advantages such as low cost, no toxicity, and high safety.[1] However, Si anodes have poor cycling behavior stemming from the large expansion (~ 300 vol%) of Si particles during their Li alloying in the lithiation stage and the corresponding contraction upon delithiation that together lead to particle pulverization, electrode delamination, and destabilization of solid-electrolyte interface (SEI) on the particle surface, leading to the drying of the electrolyte and densification of the electrode matrix. Therefore in order to alleviate the huge changes of the Si particles during cycling, some polycarboxylate polymers were mixed with the Si particles to provide cohesion with the Si particles, such as carboxymethyl cellulose (CMC), alginic acid, and poly(acrylic acid) (PAA). Among these polymers, PAA stands out with better performance. While a lot of impressive progress of silicon anodes with PAA based binders have been reported, there is insufficient understanding of factors controlling the performance of PAA in the Si-based negative electrode. To bridge this gap, one of our recent efforts is to correlate the molecular weights (MWs) of PAA binders with cycling performance, and an optimal MW range of 24 to 150 kDa was suggested for minimizing the extent of capacity fade and maintaining the cohesion in the electrode matrix despite the dramatic volumetric changes due to Si alloying.[2] Lithiation of PAA binders is another common practice for silicon lithium-ion batteries, which could benefit the large scale lamination process by enhancing the shear thinning effect. However, lithiation processes involved strong basic lithium salt, LiOH, that dramatically impact the pH values of PAA polymers. Those changes may consequently lead to some changes of the properties of PAA binders as they are pH-responsive and cause side reactions. In fact, the surface of the Si particles tend to be more easily oxidized, which led to generation of H_2.[3] It is therefore of great importance that a better understanding of the role of PAA lithiation processes should be pursued and then an optimized lithiation condition should be suggested. In this report, we aim to understand how the lithiation process and associated pH values of the PAA binder influence the cell performance of the Si/graphite composite electrodes. Such electrodes contain only ~15 wt% Si to reduce the overall expansion of the electrode during lithiation; both graphite and silicon serve as active materials in these composite electrodes.

Results

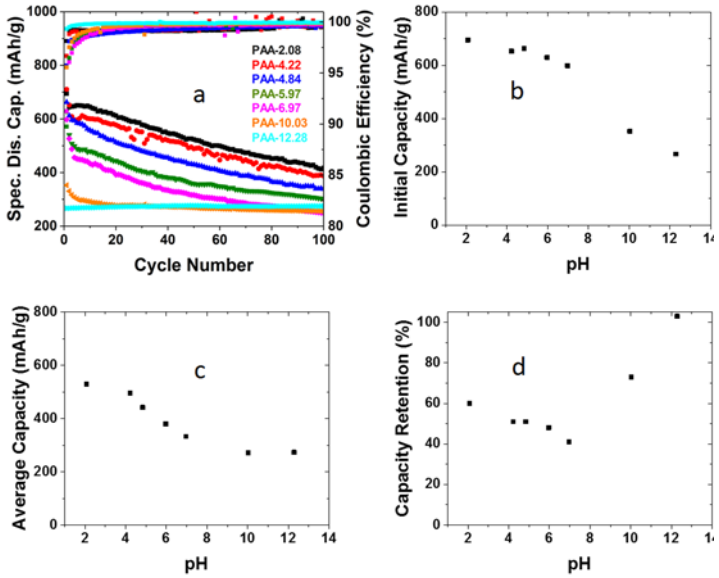

Figure 2. (a) Specific discharge capacity profiles (to the left) and coulombic efficiency profiles (to the right) of half cells using the titrated PAA samples over 100 cycles at C/3 rate; (b) (c) (d) are plots of the obtained initial capacity, average capacity and capacity retention, *vs* pH values, respectively.

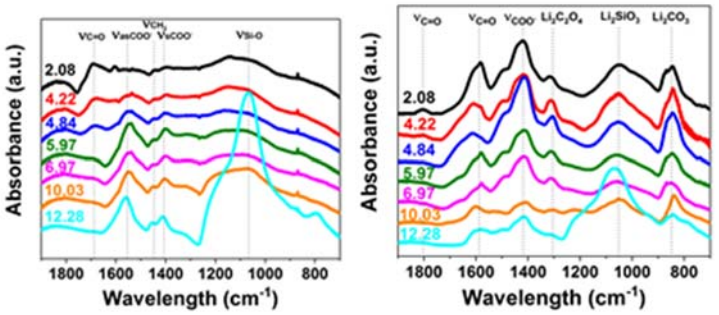

Figure 3. Fourier-transform infrared (FT-IR) spectra of the graphite/silicon electrodes containing LiPAA-1-6 before (left) and after cycling (right).

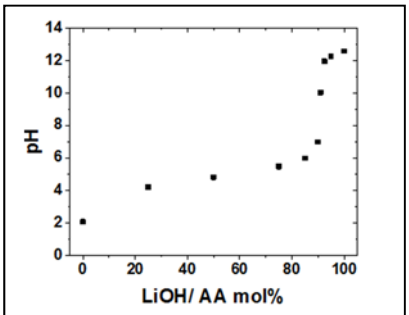

Figure 1. Plot of pH values vs lithiation percentage of the titrated PAA samples

The PAA sample with Mn of 130 kDa was used for this study. Lithiation of this sample was conducted at various ratio by titrating with LiOH solutions and the final solutions were adjusted to a constant concentration of 10% PAA. The pH values of the resulting solutions were measured using a pH meter and plotted against lithiation ratios. As shown in **Figure 1**, higher degree lithiations generally afford higher pH values. While the lower range of the lithiations (< 90%) only mildly increase the pH value from 2 to 6, slightly further lithiations (within 1%) lead to a dramatic jump from 6 to 12, where an equivalence point has been reached. After this, the pH increase is once again slowed down, only from 12 to 12.6 in the lithiation range of 90~100%. This is a typical weak acid strong base titration curve, and the 90% lithiation ratio at the equivalent point indicated that the PAA is a very weak acid while LiOH is a very strong base. The titrated samples were then used to fabricate Si/graphite electrodes and later were assembled into half cells to evaluate the cycling performance. The loading densities of these electrodes were similar around 2.7~3.0 mg/cm^2. As expected, their half cells performance was very different. From the capacity profiles (**Figure 2a**), it is obvious that the cells with less lithiated binders (lower pH value) generally afford better cycling performance. From **Figure 2b**, it is observed that for the less lithated cells with pH <7, the intial capacities are slightly decreasing as pH goes up, but comparable. Once pH values increased above 10, however, there was a huge drop from around 600 mAh/g to below 400 mAh/g. **Figure 2c**, on the other hand, showed a little different trend. For the two least lithated cells, the average capacity valuses that were obtained by averaing the capacities over 100 cycles, were on a slow decreasing slope. But this decrease was accelerated as pH went above 4. From 4 to 7, the average capacity decreased from 500mAh/g to ~320 mAh/g, a 36% drop. Further increasing of pH didn't drive the average capacity down too much. As for the capacity retention, a mild decrease was observed from pH 2 to 7. **Figure 3** shows the Fourier-transform infrared spectroscopy (FTIR) spectra of the pristine (left) and cycled (right) electrodes. In the pristine electrodes, the symmetric and antisymmetric stretching of the carboxylate ion (COO^-) at 1414 and 1562 cm^{-1}, two peaks resulting from the

lithated PAAs, decrease as pH increases. On the other hand, the C=O band at 1685 cm^{-1} decreases, which corresponds to the unlithiated PAAs. This peak essentially disappear when the pH is above 10. The broad peak at 900-1250 cm^{-1} corresponds to the Si-O band, which increases significantly under basic condition (especially for **PAA-12.28**), implying growing formations of SiO_2. For the electrodes after cycling, it is observed that all the samples had both lithiated and unlithiated PAA peaks, possibly resulting from the repeated charge/discharge cycling. More importantly, those PAA peaks decrease as pH value increases, indicating less presence of PAA binders as more lithation goes. This result may help explain the difference in the cycling performance. As more PAA binders are presented in the electrodes, a better integrity should be preserved, thus a better cycling performance should be expected.

Conclusions

The lithiation effect of PAA binders have been investigated by titrating PAA solutions with LiOH at different ratios. The resultant titration curve indicates that PAA is a weak acid while LiOH is a strong base. Those titrated binders were used to fabricate silicon/graphite composite electrodes, which were then cycled in half cells. By comparing their cycling performance, it is observed that less lithiated binders can lead to better cycling performance. FTIR results implies that less lithiated PAA binders may be more stable in the electrode matrix and cause less oxidation reactions of silicon particles.

References

1. Wu H.; Cui, Y. *Nano Today* **2012**, *7 (5)*, 414-429.
2. Hu B.; Shkrob I. A.; Zhang S.; Zhang L.; Zhang J.; Li Y.; Liao C.; Zhang Z.; Lu W.; Zhang L. *J. Power Sources* **2018**, manuscript accepted.
3. Erogbogbo F.; Lin T.; Tucciarone P. M.; LaJoie K. M.; Lai L.; Patki G. D.; Prasad P. N.; Swihart M. T. *Nano Lett*. **2013**, *13(2)*, 451-456.

Probe the relationships between functional electrolytes structure and SEI property for Si materials

Gao Liu, Tianyue Zheng (Lawrence Berkeley National Laboratory)

Background

Electrolyte decomposition products play a critical role in the stabilization of the negative electrodes in lithium-ion batteries, as the negative electrode is operated outside the stability window of the electrolyte. The electrolyte decomposition products form insoluble SEI layer, which stabilizes the electrode and electrolyte interface. Silicon alloy material has large volume expansion and surface reactions with the electrolyte when it is electrochemically lithiated. When delithiated, the Si alloy volume shrinks and surface area also decreases. This dynamic surface change causes excessive side reactions with the electrolyte. Moreover, some of the key electrolyte decomposition products are soluble in the electrolyte rather than solid precipitates. Surface coatings on Si materials by organic and ceramic have demonstrated improved surface stability towards electrolytes. Nano-sizing the Si materials can successfully prevent cracking of Si material. The Si particles are assembled by a functional polymeric binder to further improve the electrode stability in a composite electrode. We have demonstrated that both Si surface coating and functional binders can enhance cyclablity of the Si based composite electrode. Our recent development of new functional conductive binders can provide superb adhesion with the Si particle surface and allow the Si particles to expand and contract during cycling process. Surface coating on Si can prevent electrolyte interaction with the reactive surface and slow down the side reactions at the interface. The Si surface reactivity can be further reduced by tuning electrolyte and additives functions to facilitate robust SEI formation on Si materials.

Results

Pyrene (Py)-based polymers derived from 1-pyrenemethyl methacrylate (PyMA) were established as candidate electrically-conducting polymers. The flexible chain backbone of these polymers allows self-assembly of the

Py side chains into ordered structures, realizing electron conductivity via the side chain π-π stacking force of the aromatic Py moieties.[1,2] A versatile radical-based polymerization was used to synthesize PPyMA and also facilitated the incorporation of additional functional groups. For adhesion, we used the building block of dopamine methacrylamide (DMA) synthesized based on a literature procedure.[3] Poly(1-pyrenemethyl methacrylate-co-dopamine methacrylamide) (PPyMADMA) was synthesized through free-radical polymerization where the adhesive monomer, DMA, accounts for 36 mol% of this copolymer (1H- nuclear magnetic resonance spectroscopy) (Figure 1a). PPyMADMA had a number-average molecular weight of 29,000 Dalton and a polydispersity index of 1.9, while being soluble in solvents such as tetrahydrofuran (THF) and N-methylpyrrolidone (NMP). The data for PPyMA in Figure 1b and 1c were shown in our previous publication,[4] and are incorporated here for comparison. Wide-angle X-ray scattering (WAXS) results show the ordered phase characteristic of the pyrene in both PPyMA and PPyMADMA (Figure 1b). Diffraction peaks are located at ~0.95 Å-1 and ~1.02 Å-1, respectively. This corresponds to a lattice spacing of ~0.6 nanometers (nm). The broadening of the diffraction peak for the PPyMADMA sample indicates that the crystal grain size is smaller when copolymerized with DMA (Figure 1b).

To ensure that the newly-designed PPyMADMA binder still maintains the electronic conductivity, we studied the electronic structure of both the PPyMA and PPyMADMA polymers using synchrotron-based x-ray absorption spectroscopy (sXAS). sXAS is a direct probe of the excitations of core level electrons to the unoccupied valence states. Previous results demonstrate that sXAS is the tool-of-choice to reveal the critical electron state associated with the electric properties of polymer binder materials in batteries.[5,6] The methodology is based on the principle that the lowest-energy sXAS feature directly corresponds to the state of the lowest unoccupied molecular orbital (LUMO), which defines the electric properties of the polymers.[7] We also note that a comparative sXAS measurement between polymers with different functional groups is reliable without the core-hole potential concerns.[5] Figure 1c shows such a comparison of the sXAS spectra of PPyMA and PPyMADMA. The splitting peaks around 285-286 eV correspond to the π*C=C bonds with conjugation, and the features around 288 eV are from π*C=O.7 Focusing on the low-energy sXAS features corresponding to the LUMO states, it is obvious that incorporating the DMA group does not change the lowest-energy features in sXAS, indicating the LUMO of the PPyMA polymer is intact in PPyMADMA. Except for a finite change at high energies away from the LUMO states, the consistency of the overall line-shape implies that the electron states close to the Fermi level are dominated by the pyrene-based PPyMA states.

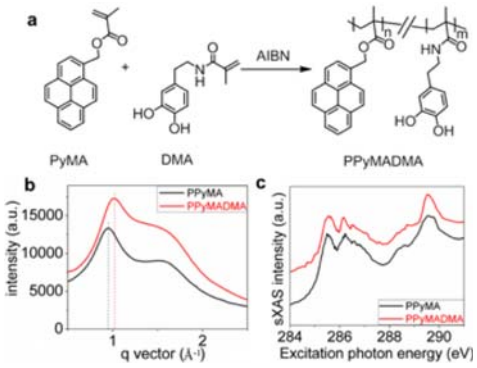

Figure 1. (a) Generic synthesis of poly(1-pyrenemethyl methacrylate-co-dopamine methacrylamide) (PPyMADMA). (b) Wide angle X-ray scattering (WAXS) of PPyMA and PPyMADMA polymers. (c) Carbon K-edge sXAS of PPyMA and PPyMADMA shows that the LUMO energy is intact in PPyMADMA, although non-conductive DMA groups are introduced.

Conclusions

Integrating chemical moieties inspired by the mussel holdfast foot protein and established side-chain conducting groups, the DOPA-containing conductive copolymer PPyMADMA was shown to be an effective binder for a Si-alloy anode in lithium-ion batteries. The facile synthetic route of the side-chain conductive polymer relaxes the requirement for synthesis and allows easy incorporation of the functional adhesion

moieties such as DOPA. Advanced synchrotron analyses of the electronic states of polymer binder reveal the pyrene moiety as the dominate electronic conductive functional groups in the copolymer, the incorporation of the DOPA moiety improves the adhesion but does not interfere with the electronic conductivities.

References

(1) Liu, F.; Xie, L.-H.; Tang, C.; Liang, J.; Chen, Q.-Q.; Peng, B.; Wei, W.; Cao, Y.; Huang, W. Organic Letters 2009, 11, 3850.
(2) Zhang, Q.; Divayana, Y.; Xiao, J.; Wang, Z.; Tiekink, E. R. T.; Doung, H. M.; Zhang, H.; Boey, F.; Sun, X. W.; Wudl, F. Chemistry – A European Journal 2010, 16, 7422.
(3) Lee, H.; Lee, B. P.; Messersmith, P. B. Nature 2007, 448, 338.
(4) Zhao, H.; Wei, Y.; Qiao, R.; Zhu, C.; Zheng, Z.; Ling, M.; Jia, Z.; Bai, Y.; Fu, Y.; Lei, J.; Song, X.; Battaglia, V. S.; Yang, W.; Messersmith, P. B.; Liu, G. Nano Letters 2015, 15, 7927.
(5) Liu, G.; Xun, S. D.; Vukmirovic, N.; Song, X. Y.; Olalde-Velasco, P.; Zheng, H. H.; Battaglia, V. S.; Wang, L. W.; Yang, W. L. Advanced Materials 2011, 23, 4679.
(6) Wu, M.; Xiao, X.; Vukmirovic, N.; Xun, S.; Das, P. K.; Song, X.; Olalde-Velasco, P.; Wang, D.; Weber, A. Z.; Wang, L.-W.; Battaglia, V. S.; Yang, W.; Liu, G. Journal of the American Chemical Society 2013, 135, 12048.
(7) Stohr, J. NEXAFS Spectroscopy; Springer Science & Business Media, 1992.

Silicon Surface Modification Using Molecular Layer Deposition

Taeho Yoon, Seoung-Bum Son, Caleb Stetson, Chunmei Ban (National Renewable Energy Laboratory)

Background

Work at NREL focuses on surface chemistry and modification to chemically or physically change the surface of electrode components, in order to improve the interphase chemistry, conductivity, and mechanical integration in Si-based electrodes. Molecular layer deposition (MLD) has been used to produce a conformal surface coating composed of an elastic metal alkoxide polymer with a tunable elastic modulus and chemical reactivity, depending on composition. The impact of the MLD coating on the electrochemical cycling performance has been in-depth investigated in FY 17 and concluded in the annual report. However, only few materials can be successfully deposted by the MLD technique, due to the requirements of the vapor pressure. Furthermore, elevated temperature is usally required during the MLD process to form conformal coating on the electrodes, which may result in the undesired interaction between the MLD precursors and the components of the electrodes. To study the fundamental roles of the surface species on the electrochemical and physical properties of the electrodes, we devoted our research to develop the liquid-phase deposition process to functionalize the silicon surface. The liquid-phase deposition are capable to explore various functional groups and can be applied for both laminated electrodes and the nanoparticles. The in-depth understanding from these studies will help establish effective mitigation to address the key challenges in Si-based electrodes; and develop strategies to deploy high-energy silicon alloys and composite electrode configurations in the full Li-ion cells.

Results

3-(aminopropyl)triethoxysilane (APTES) was deposited on the B-doped Si (100) wafer in this quarter, by using self assembled monolayer (SAM) deposition method. The illustration describing the mechanism of SAM formation is shown in Figure 1. Aminopropyl silane film is assembled on the surface of Si wafer through the formation of a Si-O-Si bond between the silanol and the surface of the Si wafer. The covalently attachment enhance the adhesion of the silane film on the surface of silicon, which ensures the coating effects during the electrochemical process.

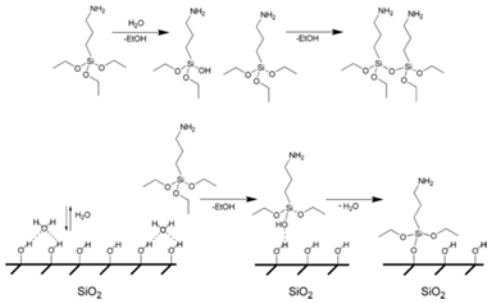

Figure 1. Reaction schemes of APTES with and without water, and the scheme for the self-assembly reaction on Si substrate.

Atomic force microscopy (AFM) has been used to characterize the surface morphology of the pristine and surface coated samples. As shown in Figure 2, surface morphology has changed after the surface treatment in terms of surface roughness. Note that the surface morphology is similar for both coated samples with 1% and 5%-APTES solutions (Fig. 2b and 2c respectively). It indicates that the conformal coating has been formed with minimum aggregation. The modified surfaces were further characterized by x-ray photoelectron spectroscopy (XPS); and the chemical composition was analyzed as well, as indicated in Figure 3. The XPS spectra from APS functionalized wafer are summarized as; (i) A well-defined peak appears at 99.2 eV in both pristine and surface-treated Si samples, due to Si-Si bond. However, the peak intensity significantly decreases in the coated sample, confirming the presence of the coating layer on the Si wafer; (ii) The peak at 284.8 eV is majorly due to the existence of hydrocarbon in the coating material. Furthermore, based on the chemical composition analysis, the carbon concentration increases significantly from 5.7% to 28.7%, after the coating. and (iii) not surprisingly, the peak representing the N-H bond appeares on the coated sample. Combining the data collected from both AFM and XPS, it is confirmed that the surface of Si wafer has been successfully functionalized by propylamine group as described above in Figure 1.

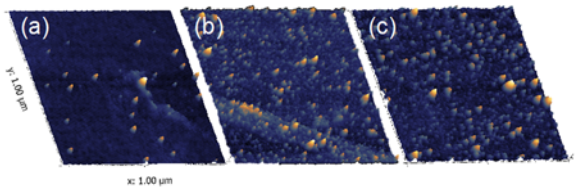

Figure 2. AFM images of (a)pristine Si wafer, (b) Si wafer treated with the 1% APTES solution, and (c) Si wafer treated with 5% APTES solution.

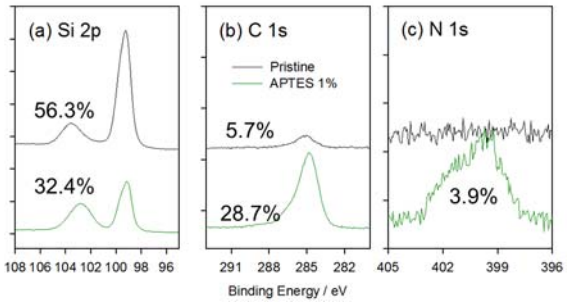

Figure 3. XPS spectra of (a) Si 2p, (b) C 1s, and (c) N 1s of the pristine sample and the samples treated with the 1% APTES solution.

The impact of the APTES coating on the electrochemical behavior has been demonstrated, as shown in Figure 4. Two electrolytes, including 1.2 *M* $LiPF_6$ in EC:EMC=3:7 (GEN2) and FEC-added electrolyte (GEN2 with 10% FEC), have been used. Interstingly, there is negligible difference between the pristine Si and the coated Si electrodes. The coulombic efficiencies (CE) of the pristine and APTES-treated electrodes are slightly different, which are 94.5 and 94.1% respectively. Lower values in CE are observed when using FEC-added electrolyte, because of the reduction of the FEC additive. However, the coated Si electrode shows higher CE (92.4%) than that of the pristine electrode (87.3%), which implies the effect of the aminopropyl silane coating on the electrochemical reversibility. Research including electrochemical impedance spectroscopy, FTIR and XPS is ongoing and will be summarized in next report.

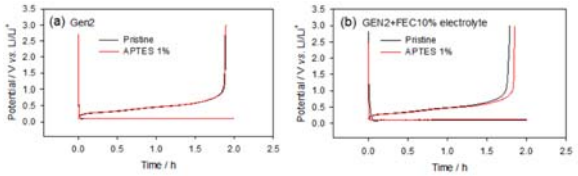

Figure 4. Voltage profiles of pristine and surface-treated Si samples in FEC-free electrolyte (1.2M LiPF6 in EC:EMC 3:7) and FEC-added electrolyte (1.2 M $LiPF_6$ in EC:EMC 3:7 with 10% FEC).

Conclusions

Liquid deposition was developed and applied for the preparation of the aminopropyl silane coating for silicon wafer electrode. XPS and AFM have been used to characterize the coating chemistry and morphology. The preliminary data collected from the electrochemical lithaition and delithiation show no much difference on the electrochemical reversibility for the first cycle. However, the coating improves the reversibility in electrochemical reaction when FEC was used as an additive. With the view of these finding, we are investigating the coating effects by using electrochemical impedance spectroscopy and FTIR, to identify the interaction between the FEC and surface coating layer and determine the coating effects on electrochemical and physical properties in the silicon electrode.

Interfacial Modification of Si Anode for High Energy Li-ion Battery

John Zhang (Argonne National Laboratory)

Background

In this quarter, we continue to research the surface modification of silicon particles by electrochemical approach and organic synthesis approach. The former is to design new electrolyte/additive that could chemically/electrochemically decomposes and deposits on the lithiated Si surface forming a resilient SEI layer that stabilizes the interfacial reactivity of LixSi and electrolyte. Fundamental understanding of how the reactivity of electrolyte/additive with Si anode and how the chemical composition of SEI affects the cell

performance will be systematically performed. Another approach is proposed to functionalize the surface of Si particles through organic silane chemistry forming an artificial SEI for improved performance.

FEC is considered as the best performing electrolyte additive for Si anode. In this quarter, new fluorinated carbonates were studied as additives and their performance in Si/Li half cells were compared with FEC. For the Si particle surface modification, we continue to explore the impact of other surface functionalities on the electrochemical performance of Si.

Results

1. Fluorinated Carbonates Additives

Two new additives based on fluorinated carbonate compounds difluoroethylene carbonate (DFEC) and fluorinated propylene carbonate (TFPC) were studied as additive for Si anode during the electrochemical formation process. Different from FEC, DFEC has two fluorine substitution on the two ethylene carbon atoms and TFPC has a fully fluorinated methyl substitution. It is our great interest to examine how effective of these fluorinated carbonates on the electrochemical performance in Si anode compared with FEC. **Figure 1a** shows the first cycle voltage profiles for Si/Li half cells using electrolyte Gen2+10% DFEC, Gen2+10% TFPC and compared with Gen2+10% FEC. No new plateaus in voltages profiles were observed for DFEC and TFPC additives and the same results was obtained from the differential capacity profiles (dQ/dV) of these threes cells (**Figure 1b**). Same at the FEC additive, the DFEC and TFPC cells didn't show the crystalline $Li_{4.4}Si$ phase after the 1st formation cycle in the delithiation process, which is quite different from our previous reported FEC/HMDS dual additive cell. As shown in **Figure 2**, the result has been repeated for multiple times in testing. Obviously, the chemical structure and the number and nature of the fluorination groups play a significant role in the SEI formation. It is not our intention to deeply understand its failing mechanism. Instead, our strategy is to continue explore new additives and new electrolyte formulations which could enhance the cycling performance of the Silicon anode. New fluorinated electrolyte research in ongoing.

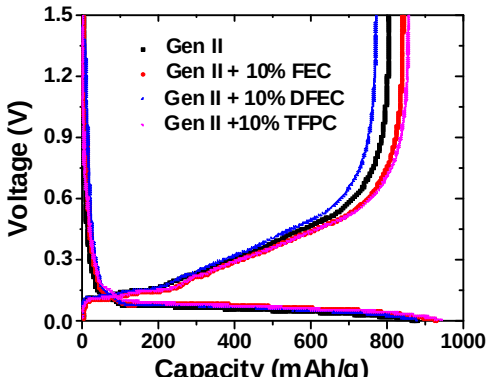

(a)

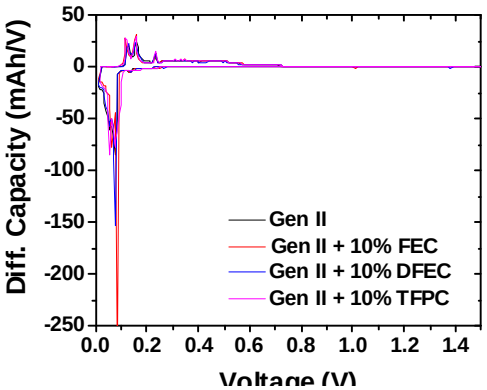

(b)

Figure 1. (a) The 1st cycle voltage profiles for Si-graphite/Li half cells using Gen2, Gen2+10% DFEC, Gen2+10% TFPC and Gen2+10% FEC (the baseline electrolyte), and (b) dQ/dV profiles for the 1st cycle for the Si-graphite anode with Gen2, Gen2+10% DFEC, Gen2 +10% TFPC, and Gen2+10% FEC (the baseline electrolyte).

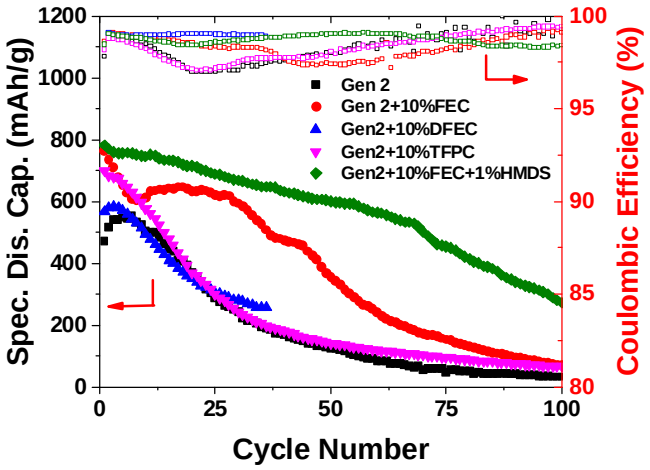

Figure 2. Capacity retention and Coulombic efficiency of Si-graphite/Li half cells with Gen 2 electrolyte, Gen2+10% DFEC, Gen2+10% TFPC and Gen2+10% FEC.

2. Si Particle Surface Functionalization

Silanol (Si-OH) surface enriched Si nanoparticles were synthesized and used as reaction platform for new functional amine (-NH_2) and epoxy (OCH_2CH-) group attachment. **Figure 3** depicted the synthetic procedure of the Si nanoparticles with aminopropyl triethoxysialne (APTES) and glycidoxypropyl trimethoxysilane (GPTMS), respectively.

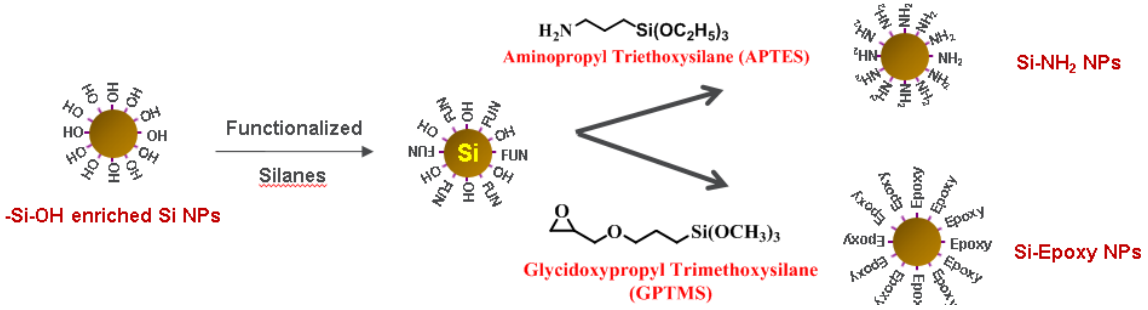

Figure 3. Synthesis of Si nanoparticles with amine and epoxy functionality.

FTIR was used to confirm the existence of the surface functionalities. New peaks around 2800 – 2900 cm^{-1} for both samples are the typical C-H stretching vibration of -CH_2CH_2- group. As for the Si-NH_2, a typical vibration peak for primary amine (1560 cm^{-1}) was observed. And for the Si-Epoxy, the peak around 1250 cm^{-1} corresponds to the epoxy ring. We also compared the FTIR spectra of the silane precursor s the corresponding functionalized silicon NPs. The overlap of the typical bands of the functionalized SiNPs and their silane

precursors is a further evidence that the surface functionalization is successful. **Figure 4** shows the TGA profiles. The –Si-OH enriched Si NPs lost 1.5 % weight at 800 °C, while 3.5% and 2.5% for Si-NH_2 and S-Epoxy, respectively. The difference in weight loss further confirms the successful attachment of the functional groups.

The anode electrode was prepared with 70% surface functionalized Si-NH_2 and Si-Epoxy particles, 10% Timcal C45 and 20% PAA aqueous solution, which was then evaluated with 2032 coin cells. The electrolyte is Gen 2 with 10% FEC. Charge-discharge cycling was performed between 0.01-1.5 V with a current rate of C/3 following three formation cycles at C/20.The preliminary cycling data indicates the epoxy functionalized Si NPs showed improved performance than that of the baseline anode, silanol (-SiOH) enriched NPs and the amine functionalized (Si-NH_2) NPs. This is the first surface functionalized Si NP sample that demonstrated its effectiveness in promoting its electrochemical performance. This result is encouraging and motivates us for extensive future screening research.

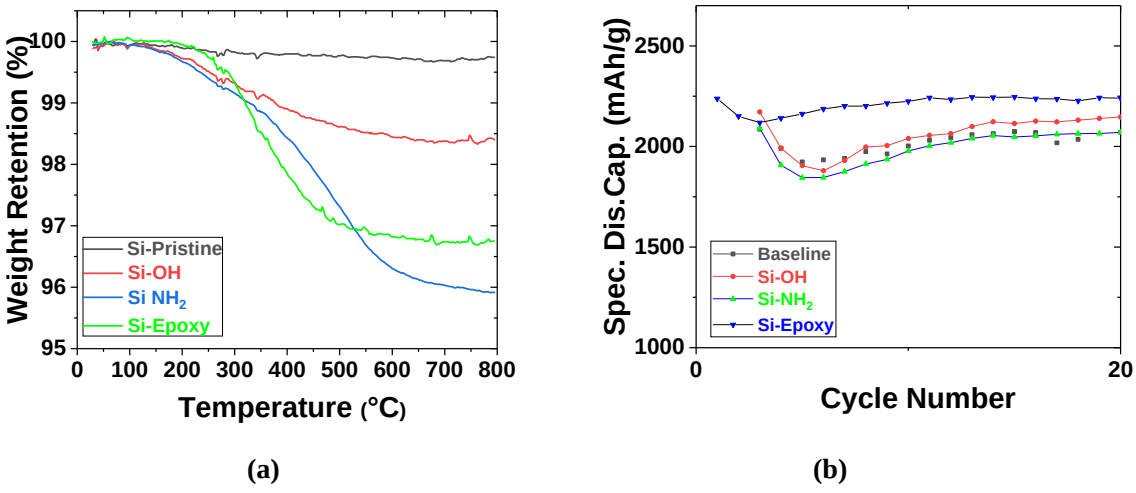

Figure 4. (a) TGA profiles of (i) baseline Si NPs, (ii) Si-OH NPs, (iii) Si-NH_2 NPs and (iv) Si-Epoxy NPs, and (b) capacity retention of Si/Li half cells with baseline Si, Si-OH NPs, Si-NH_2 NPs and Si-Epoxy NPs.

Development of High Energy Metals

Wei Tong (Lawrence Berkeley National Laboratory)

Background

Amorphous Si-Sn films with Sn < 40 mol% was determined to be ideal compositions in thin film batteries, for example, $Si_{0.66}Sn_{0.34}$ showed a large reversible capacity of ~ 1900 mAh/g and low irreversible capacity of ~ 100 mAh/g during the 1st cycle. In-situ XRD studies revealed that the amorphous feature remained upon cycling. More specifically, the local tetrahedral arrangements of Si, Sn atoms in amorphous $Si_{0.66}Sn_{0.34}$ are similar to those in $Li_{4.4}Si$ and $Li_{4.4}Sn$, with Si/Sn on the corners and Li in the center. Therefore, the excellent cycling behavior was attributed to the potential elimination of two-phase regions between phases of different Li content in amorphous material, leading to homogeneous volume expansion.[1] Ahn *et al.* later confirmed that amorphous Si-Sn nanocomposite film electrodes produced by magnetron co-sputtering method demonstrated improved cycling performance compared to amorphous Si film at a similar thickness.[2] Sputtered films with separated amorphous Si embedded in the Sn matrix also delivered a reversible capacity of 1400 mAh/g with good cycling stability at Si/Sn ratio close to 1.[3] However, evidence of amorphous Si and Sn phase separation was revealed in both work, which was consistent with their immiscibility. In this project, we propose to

employ the scalable splat quenching approach to prepare amorphous Si-Me (Me is metal) materials and improve the structural stability of the host Si electrode.

Results

Splat quenching method was extensively used in metallurgy, but not in battery field. In the first quarter, we conducted a literature survey to review the previous reports on amorphous Si-based metal/alloy systems. Our literature review focused on two aspects, including amorphous Si-Me systems for Li-ion batteries as well as preparation of amorphous Si-Me materials by splat quenching method. In the latter, particular attention was paid to the phase formation and synthetic conditions as well as their effects on a variety of properties (e.g., crystallization temperature, electrical conductivity etc.) that are most relevant to our future material design and preparation in this project. Of note, higher crystallization temperature is favorable for the preparation of amorphous phases.

Various Si-Me based thin films were prepared by magnetron sputtering method to explore their electrochemical behaviors in the Li-ion batteries. A number of amorphous Al-Si-Me (M = Fe, Ni, Cr, Mn, Fe-Ni, Fe-Co) systems were prepared by melt-spinning method. The amorphous range is 12 – 42% Si and 8 – 23% Me in $Al_{90-x}Si_xMe_{10}$ (Me = Cr, Mn, Fe, Co, Ni).[4] In addition, the crystallization temperature significantly varies with Me in $Al_{75-x}Si_{25}Me_x$ systems. Crystallization temperature increases with Me content, 10% increase in Me can lead to an increase of ~ 200 ^{0}C in crystallization temperature. Meanwhile, lower crystallization temperature was observed for Ni and Co (low content) compared to Mn, Cr, and Fe. On the other hand, effect of Si content on crystallization temperature is minimal compared to Me, a difference of 50 ^{0}C in crystallization temperature was observed with Si content increasing from 10 to 40% in $Al_{85-x}Si_xMe_{15}$ systems. In contrary, electrical conductivity of the final products varies less with Me content, except Co, increase in Co content led to a significant decrease in electrical conductivity. Electrical conductivity increases with Si at lower Si content (< 20%), but remained quite constant at higher Si content.[5] The phase evolution and electrochemical behavior of Si-Al-Mn thin films in a wide composition range were reported. Amorphous film formation in a wide composition range was revealed, but Mn content had a large effect on electrochemistry. Irreversible specific capacity increased with Mn content but remained fairly low (10 – 15%) for composition with about 10 atom% Mn. Meanwhile, increasing Mn content led to a decrease in discharge capacity. The best composition of Si-Al-Mn within the range that can be melt-spun amorphously was determined to be $Si_{0.42}Al_{0.44}Mn_{0.14}$, corresponding to the maximal Si content with Mn content of ~ 10 atom%.[6] Attempts were made to prepare amorphous Al-Si-Mn alloys by melt-spinning method. However, the final products exhibited either crystalline phases such as Si, Al or a large irreversible capacity (~ 30%), which is quite different from those in thin films.[7]

Other relevant work was done on $Si_{1-x-y}Sn_xMM_y$ (MM is a mixture of rare earth elements). The goal is to bond Sn to MM in preference to Si and suppress crystalline Sn formation. Moreover, the addition of cerium and lanthanum-rich metals is expected to increase crystallization temperature of the amorphous $Si_{1-x-y}Sn_xMM_y$ alloys, making their preparation in the amorphous state more possible by melt-spinning method. Addition of MM decreases specific capacity. Amorphous $Si_{1-x-y}Sn_xMM_y$ phases developed at Sn content of 20 – 40% and MM content of 15 – 20%. An optimal composition of $Si_{0.52}Sn_{0.35}MM_{0.13}$ delivered a specific capacity of 1000 mAh/g with good capacity retention. Phase formation in Si-Sn-Ti system prepared by arc melting method was also explored.[8] A ternary Si-Sn-Ti phase with tetragonal W_5Si_3 structure type and *I*4/*mcm* space group was identified in Ti-rich region along with Si-Ti, and Sn-Ti binary phases.[9]

Conclusions

Splat quenching method is scalable and suitable for amorphous phase preparation, can potentially address the challenges in sample holder, homogeneous mixing, and oxide contamination. In the next quarter, we will set up and start testing our newly purchased splat quencher. From the literature survey, proper parameter control in a suitable composition range is necessary to produce amorphous materials. We will combine thin film sputtering and splat quenching techniques to produce promising Si-Me compositions (e.g. Al, Mn, Ti, Sn etc).

References

1 Beaulieu, L. Y. *et al.* The Electrochemical Reaction of Li with Amorphous Si-Sn Alloys. *J. Electrochem. Soc.* **150**, A149-A156, (2003).

2 Ahn, H.-J., Kim, Y.-S., Park, K.-W. & Seong, T.-Y. Use of Sn-Si nanocomposite electrodes for Li rechargeable batteries. *Chem. Commun.*, 43-45, (2005).

3 Xiao, X. *et al.* Phase-separated silicon–tin nanocomposites for high capacity negative electrodes in lithium ion batteries. *J. Power Sources* **214**, 258-265, (2012).

4 Inoue, A., Bizen, Y., Kimura, H. M., Masumoto, T. & Sakamoto, M. Compositional range, thermal stability, hardness and electrical resistivity of amorphous alloys in Al-Si (or Ge)-transition metal systems. *J. Mater. Sci.* **23**, 3640-3647, (1988).

5 Dunlap, R. A. & Dini, K. Amorphization of rapidly quenched quasicrystalline Al-transition metal alloys by the addition of Si. *J. Mater. Res.* **1**, 415-419, (2011).

6 Fleischauer, M. D. & Dahn, J. R. Combinatorial Investigations of the Si-Al-Mn System for Li-Ion Battery Applications. *J. Electrochem. Soc.* **151**, A1216-A1221, (2004).

7 Sun, Z. B. *et al.* Electrochemical properties of melt-spun Al–Si–Mn alloy anodes for lithium-ion batteries. *J. Power Sources* **182**, 353-358, (2008).

8 Dahn, J. R., Mar, R. E., Fleischauer, M. D. & Obrovac, M. N. The Impact of the Addition of Rare Earth Elements to Si1 − x Sn x Negative Electrode Materials for Li-Ion Batteries. *J. Electrochem. Soc.* **153**, A1211-A1220, (2006).

9 Zhan, Y., Yang, W., Xu, Y. & Zhang, X. Experimental phase diagram of the Ti–Si–Sn ternary system at 473K. *J. Alloys Compd.* **509**, 5269-5273, (2011).

Si anodes with extended cycle life and calendar life

Ji-Guang Zhang, Xiaolin Li (Pacific Northwest National Laboratory)

Background

Nano Si or highly porous structured Si has been widely used to avoid pulverization of Si particles during cycling process. However, large surface area of nano Si or micron sized porous Si may also lead to a continuous reaction between lithiated Si and electrolyte. As a result, this reaction may lead to continuous growth of SEI layer and increase of cell impedance. Another possible degradation mechanism is the cross talk between Si anode and cathode. The mitigation of dissolved Mn in cathode may poison Si anode; FEC additive which is highly effective in forming a stable SEI layer on Si may form a detrimental cathode electrolyte interface (CEI) on cathode surface which also leads to impedance increase. Therefore, minimize the surface area of Si and find a stable electrolyte additive are critical for long term stability of Si based Li-ion batteries.

In this project, we will enhance the cycle life and calendar life of Si based Li-ion batteries by designing a stable porous Si structure and develop an artificial SEI layer coated on the surface of porous Si particles. A more stable electrolyte additive or solvent mixture will be developed to minimize the detrimental effect of FEC currently used in Si based Li-ion batteries. The degradation mechanism of Si anodes during shelf storage will be systematically investigated. New insight on these mechanisms and the new approaches developed in this work will speed up the deployment of high energy Li-ion battery with Si-based anodes and increase market penetration of EVs and PHEVs as required by DOE/EERE.

Results

In this quarter, the electrochemical performances of Si/MWNT/C composite with different mass loadings as well as the full cell have been investigated. The electrodes with different areal mass loadings were evaluated, as shown in Figure 1. In the case of the active material mass loading of 1.68 mg cm^{-2}, the reversible areal capacity reaches 2.6 mAh cm^{-2} at the current density of 0.2 mA cm^{-2} (after 3 formation cycles). Following deep cycling at a higher rate of 0.7 mA cm^{-2}, the capacity retention is 80% (vs. the 4th cycle) after 80 cycles. At slightly lower mass loadings of 0.94 mg cm^{-2} and 0.45 mg cm^{-2}, nearly no capacity fade was observed up to

100 and 150 cycles, respectively. The average specific capacity of the high-mass-loading electrode is 1450 mAh g^{-1}, which is similar to that of the thinner electrodes, suggesting that almost all microspherical silicon composite is active in the thick electrode. We can attribute this promising cycling stability to the well-designed hierarchical structure, which provides (1) enough void space to accommodate the volume change so that the swelling of the composite can be reduced; (2) good mechanical structure and electronic conductivity from the MWNT matrix.

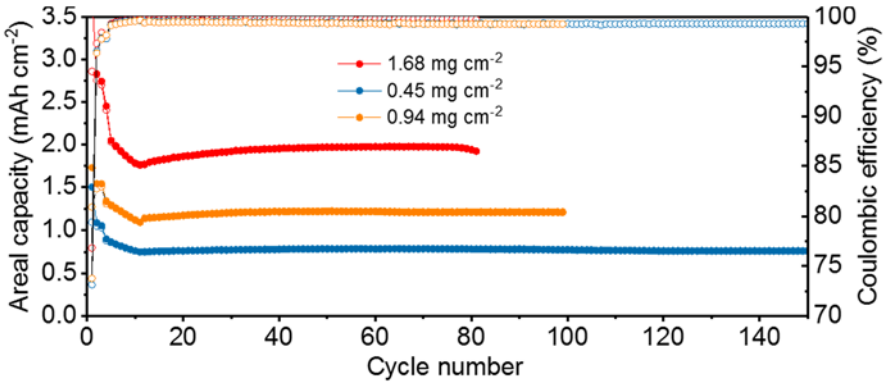

Figure 1. Long-term cycling performance of Si/MWNT/C composite with different mass loadings.

NMC333 was selected as the cathode materials to match with Si/MWNT/C anode for full cell study. The anode was pre-cycled against Li metal in half-cells before re-assembled into full cells. The actual capacity ratio of Si anode to NMC cathode is 1.2:1, which suggests higher Si content is favorable to prevent the anodes from over-lithiated during full-cell charge. The cycling performance of the full cell is measured with a voltage window range from 2.7 to 4.3 V, and the capacity of full cell is calculated based on the total mass of Si/MWNT/C and NMC. An initial discharge capacity of 140 mAh g^{-1} was obtained with the first Coulombic efficiency of 84.98%. Good capacity retention of ~91% after 100 cycles was demonstrated.

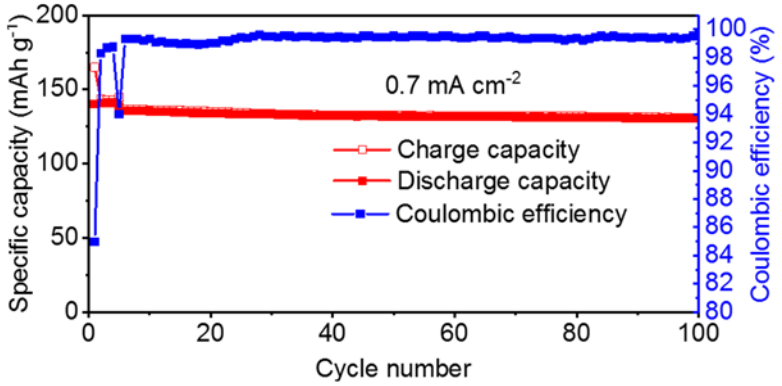

Figure 2. Long-term cycling performance and Coulombic efficiency of Si/MWNT/C//NCM full cell at 0.7 mA cm^{-2} (0.2 mA cm^{-2} for the first three formation cycles)

Conclusions

The hierarchically structured Si/MWNT/C demonstrates good long-term cycling performance even with high areal mass loading. The electrodes deliver an average reversible capacity of 1.92 mAh cm^{-2} after 80 cycles. Full cell of Si/MWNT/C//NCM exhibited stable cycling performance with a capacity retention ratio of 91%.

References

1. Hierarchical-structured, silicon-based electrodes and methods of making same, Haiping Jia, Ji-Guang Zhang, and Xiaolin Li, U.S. patent filed on Nov. 2017.

Hydro/Solvothermal Synthesis and Scale-up of Silicon and Silicon-containing Nanoparticles

Youngho Shin, Gregory K Krumdick (Argonne National Laboratory)

Background

The immediate objective of this project is to develop and set up an advanced bench-scale hydro/solvothermal synthesis system for the production and evaluation of high-capacity engineered silicon nanoparticles and composites used as the active anode material in Li-ion batteries. These materials need to be tested and validated in large format prototype cells before going to high-volume manufacturing which use a fair amount of material. For this reason, the synthetic capability to be developed would be based on the design and construction of a turnkey hydro/solvothermal synthesis reactor system capable of batch production of 10 to 50 g of nanoparticles per run.

One of the features of the present process is to provide a bottom-up synthesis approach (stacking atoms onto each other) of silicon nanoparticles and composites which is more advantageous than the common top-down synthesis approach (etching out crystals planes) because the former has a better chance of producing nanostructures with less defects, more homogenous chemical composition, and better short- and long-range ordering. Using this advanced bottom-top synthesis approach, the crystallinity, particle shape and size of silicon nanoparticles incorporated into their composites, which are the key parameters of these materials' failure, should be intensely investigated and optimized to support the fundamental understanding of the EERE-VTO Energy Storage Si Deep Dive projects.

Results

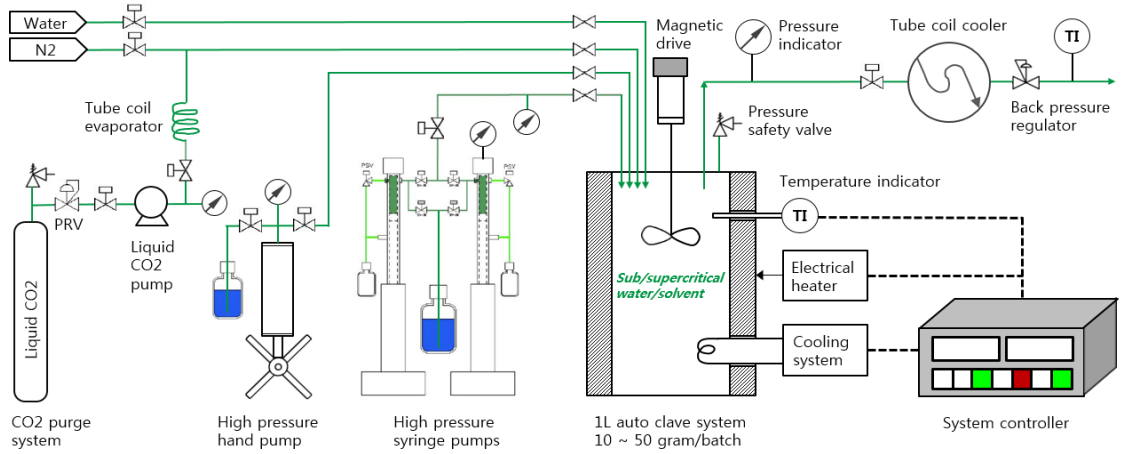

Figure 1. Schematic diagram of bench-scale hydro/solvothermal synthesis reactor system

Hydro/solvothermal synthesis is generally defined as crystal synthesis or crystal growth under high temperature and high pressure with water or organic solvent as the reaction medium and utilizing precursors that are ordinarily insoluble in water [1-2]. The formation of nano-sized materials can be achieved in supercritical water (SCW) and subcritical water (SbCW) because of the high reactant diffusivity, fast reaction rates, and extremely high nucleation rate of these novel reaction media. As a result, hydro/solvothermal reactors can generate highly crystalline nano-sized particles with well-defined morphology and tuned particle

size distribution. This hydro/solvothermal process became the first commercial factory in the world at 2010 for lithium iron phosphate production led by Youngho Shin [3]. Based on this demonstrated promise, a bench-scale hydro/solvothermal synthesis reactor system for silicon nanoparticles and composites was designed and is currently undergoing installation as shown in Figure 1.

Using the developed process, we will obtain silicon nanoparticles (50 ~ 200 nm) with narrow particle size distributions. The particle size of silicon can be controlled by adjusting the density of reaction media which depends on the reaction temperature and pressure. Also the morphology and crystal structure of silicon nanoparticles can be improved by changing organic modifiers to achieve better battery performance. Figure 2 shows some synthesis schemes to generate silicon nano-particles using the reactor system to be installed [4-5].

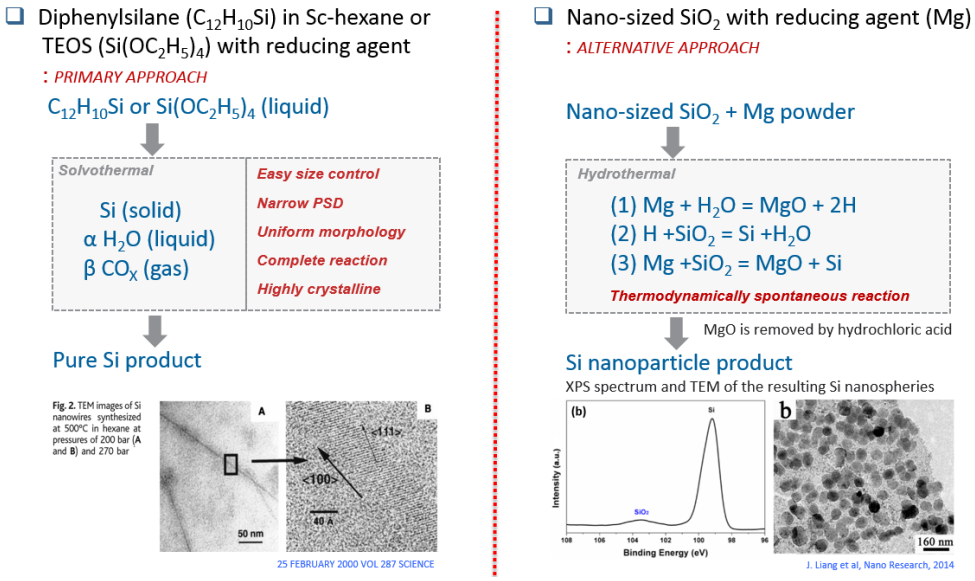

Figure 2. Silicon nanoparticle synthesis approaches using hydro/solvothermal reactor system

Conclusions

An advanced hydro/solvothermal synthesis reactor system capable of batch production of 10 to 50 g per run will be installed at the end of the third quarter of FY18 which will provide a bottom-up synthesis approach of silicon nanoparticles and composites. Using the developed process, silicon nanoparticles will be prepared and delivered to collaborators for testing and validating in large format prototype cells.

References

[1] Murukanahally Kempaiah Devaraju, Quang Duc Truong, Hiroshi Hyodo, Takaaki Tomai and Itaru Honma, Inorganics, 2 2014, 233-247.
[2] Youngho Shin, S.-M. Koo, D.S. Kim, Y.-H. Lee, B. Veriansyah, J. Kim and Y.-W. Lee, J. Supercrit. Fluids 50, 2009, 250.
[3] Tadafumi Adschiri, Youn-Woo Lee, Motonobu Goto and Seiichi Takami, Green Chemistry 13, 2011, 1380.
[4] Justin D. Holmes, Keith P. Johnston, R. Christopher Doty and Brian A. Korgel, Science Vol 287, 25, 1471-1473, 2000
[5] Jianwen Liang, Xiaona Li, Yongchun Zhu, Cong Guo and Yitai Qian, Nano Research Vol 8, 5, 1497–1504, 2015

Lithium Inventory

C. S. Johnson and W. M. Dose (Argonne National Laboratory)

Background

Over-lithiated $LiNiO_2$, or Li_2NiO_2, has extra lithium in its structure which may be used as sacrificial lithium additive. The technology has been proposed for use with high-capacity SiO_x anodes in lithium-ion batteries [H. Park et al. Electrochim. Acta, Vol. 108, 591-595 (2013)]. The first cycle irreversible loss problem at the SiO_x anode was addressed with this approach. The second equivalent of Li from Li_2NiO_2 is removed from the cathode material during a first charge leaving an amorphous $LiNiO_2$ that is then cycled along with the majority active material cathode. In principle this is a viable method to supply lithium to a cell such that lithium inventory is better controlled and/or improved. In this work we evaluate whether this mechanism could be applied to NMC532 or $Li_{1+x}NMCO_2$ as the over-lithiated phase to boost the cyclable lithium or lithium inventory in the cell. The structural change upon over-lithiation is measured, and the electrochemical testing was conducted on this system this past quarter.

Results

Our previous work employed a thick $LiFePO_4$ counter/reference electrode as a large reservoir supply of lithium for the 15%Si-graphite cell. We found that the capacity degrades mainly in the Si component first, then later in the graphite portion suggesting that the graphite also is affected by (de)lithiation Li_xSi volume changes or possibly another mechanism. The thick $LiFePO_4$ together with its flat voltage plateau and structure stability allowed us to cycle the cell to 1000 cycles thus completing a full assessment of the behavior of the lithium and its inventory change.

This quarter we cycled different loadings of 15%Si-graphite/$LiFePO_4$ full cells in order to better assess the lithium inventory changes seen in the Si-graphite blended electrode. The n/p ratios of the cells were excess Li (n/p = 0.26; black markers), slight excess of Li (n/p=0.98; red markers), and limited Li (n/p=1.5; blue markers). In this experimental design, the cells are cycled to a capacity or voltage limit with the following conditions: charge = 600 $mAhg^{-1}$ or 4.455 V, discharge to 2.0 V; C/10 rate, 30 °C, with Gen 2 electrolyte and 10% FEC additive.

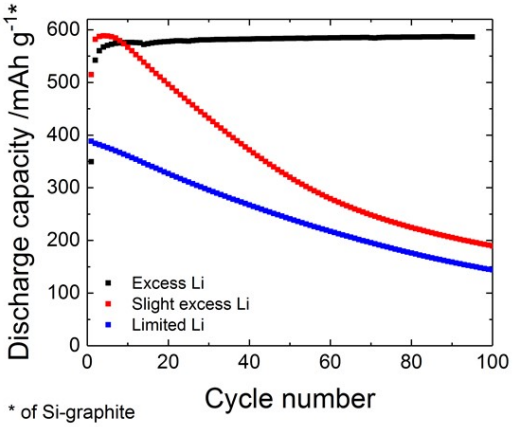

Figure 1. 15%Si-graphite/$LiFePO_4$ full cells cycling performance to 100 cycles. Cycling conditions are described in the body text. Black markers are cell design with excess Li; red markers are slight excess of Li in the cell, and blue is limited Li in the cell.

Figure 1 is a plot of the discharge capacity as a function of the cycle number (out to 100 cycles). Having sufficient Li inventory gives rise to stable cycling (black data markers) and delayed capacity fade. For insufficient lithium (or once excess Li present is consumed) then instead, it gives rise to rapid capacity fade. Since the result in Figure 1 demonstrates that the presence of extra Li present helps the cyclability of 15%Si-graphite electrode, we try to envision different ways to introduce extra lithium into the cell in a straight-forward way. Thus, we hypothesize that an over-lithiated $LiNMCO_2$ could also be a route to introduce lithium inventory into the cell.

To explore this concept further, half cells of $Li/LiNMCO_2$ (NMC = 532) were built and discharged first to 1.1 V. About 127 $mAhg^{-1}$ (C/10 rate) was obtained as shown in Figure 2a. The structure indeed can accommodate extra lithium. If the cell is charged first to 4.5 V, then discharged to 1.1 V, an extra 104 $mAhg^{-1}$ results (Figure 1b). The inset in Figure 1b shows that the open circuit voltage around 1.555 V remains constant indicating an electrochemically stable material. Therefore, the NMC532 has the capability to store more lithium in its structure to roughly a nominal stoichiometry of $Li_{1.4}NMCO_2$. In principle the extra lithium in the structure (0.4Li) will not add much weight to the overall electrode for practical operation.

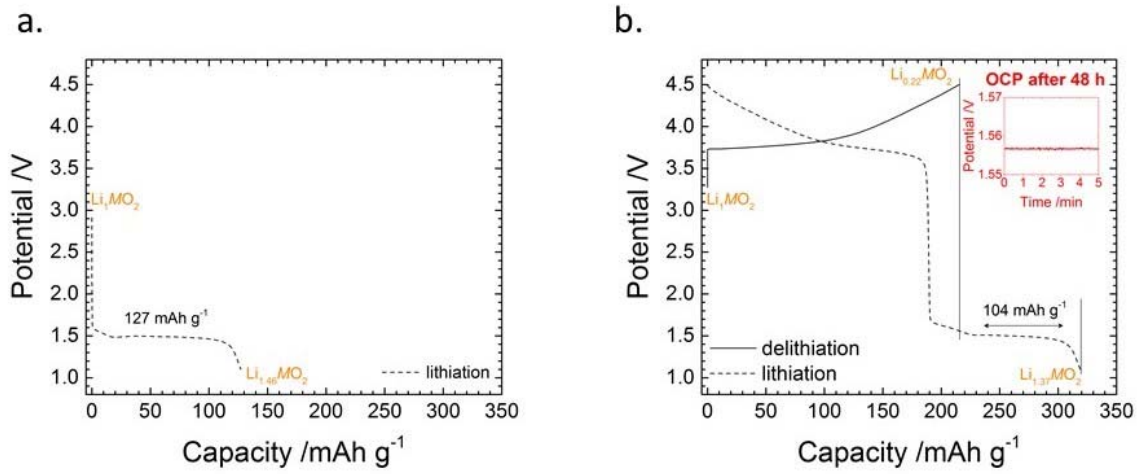

Figure 2. (a) $Li/LiNMC532O_2$ discharge first, and (b) charge to 4.5 V, then discharged to 1.1 V at C/10 rate. The inset is a measurement of the OCV taken 48 h after discharge step to 1.1 V.

From X-ray diffraction data, the results clearly show that a nominal di-lithium Li_2NMCO_2 crystalline phase is formed. For the di-lithium phase, the extra lithium is known to go into the adjacent tetrahedral sites in the Li layer [C. S. Johnson et al., Chem. Mater. Vol. 15, 2313 (2003)]. However, at this moment, it is not clear how the di-lithium phase is integrated into the parent $LiNMCO_2$ phase and what its precise stoichiometry is. Nevertheless, the extra lithium and its effect on the cycling characteristics in Li half cell over 100 cycles was carried out. Figure 2b shows that the over-lithiation step (Fig. 2a) is detrimental to the cycle performance of the material when cycled in normal voltage window of 3.0 to 4.5 V. The blue markers (Fig. 2b) clearly indicate a substantial capacity fade compared to the control (black markers; Fig. 2b). It could be that the over-lithiation step is too damaging to the bulk structure, leaving an irreversible or kinetically sluggish phase. We also performed slow cycling (C/100) and holds (@ 3.0 V for 12 h), but still the capacity drastically drops over 100 cycles.

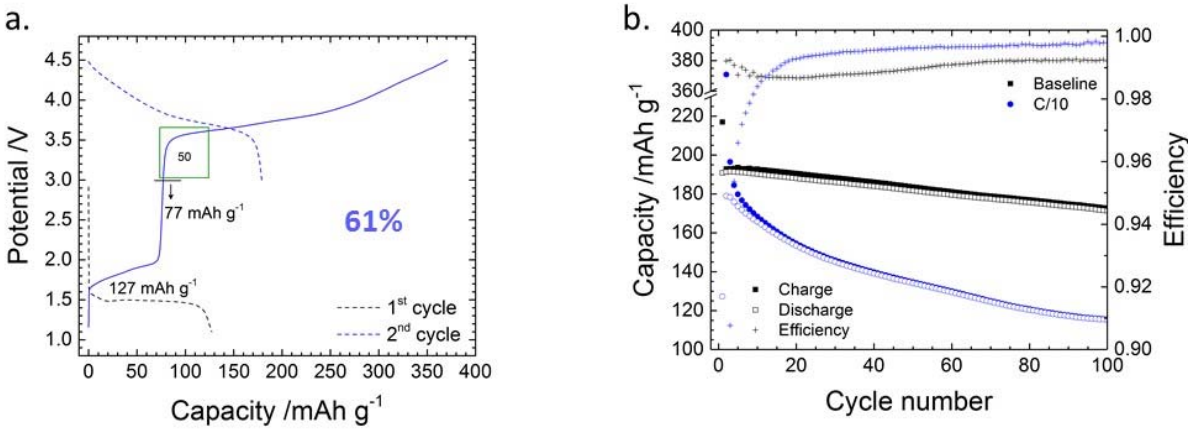

Figure 3. (a) Li/LiNMC532O_2 discharge first, then subsequent charge to 4.5 V, and discharge down to 3.0 V, and (b) cycle performance of the cell formed in (a) over 4.5 to 3.0 V only for 100 cycles at C/10 rate (blue), and a control cell Li/NMC532 between 4.5 to 3.0 V (no low voltage cycle). The current rate is C/10.

Not only was the di-lithium phase seen by X-ray diffraction methods, the oxidation state of all the transition metals, Mn, Ni, and Co were reduced as confirmed by XANES measurement for the electrochemically over-lithiated NMC532. The results are shown in Figure 4a-c for Mn, Co and Ni K-edges respectively. It is feasible that the over-lithiation causes strong structural distortions in the local MO_6 octahedra as Jahn-Teller Mn(III) and Co(II) cations are formed. Conceivably local structural distortion could be cooperative which could lead to irreversible bulk crystal fractures, and subsequent capacity fade in a lithium cell.

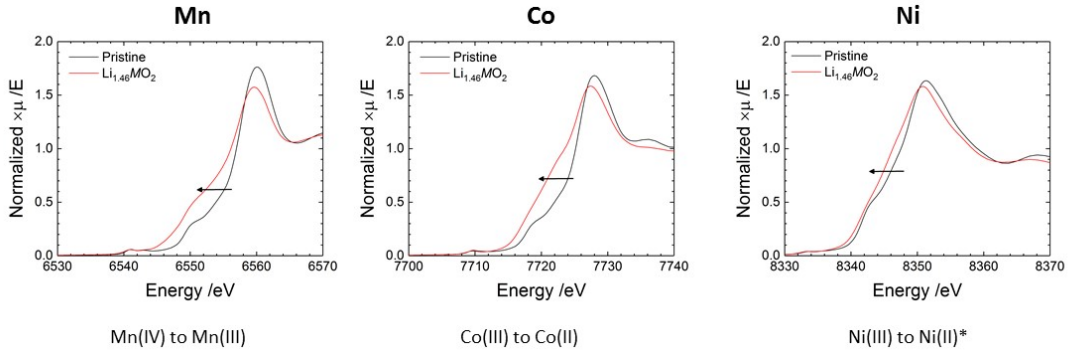

Figure 4. The XANES spectra for nominal $Li_{1.4}NMCO_2$ from electrochemically over-lithiated process. It is clear that all the metals' redox states are reduced upon over-lithiation. (measurement courtesy of Drs. Soojeong Kim and Tim Fister).

Conclusions

Demonstration of thick $LiFePO_4$ cathode in conventional CAMP-produced 15%Si-graphite cells (A11 electrodes) showed that extra lithium (high lithium inventory) is critical to successful operation of this cell chemistry. It is feasible that lithium housed in $LiNMCO_2$ in over-lithiated state could also provide the necessary extra lithium in the cell without much electrode weight gain. First over-lithiated NMC532 (i.e. $Li_{1+x}NMCO_2$) was evaluated for its reversibility in Li half cells. Results show that formation of this phase (at low voltage) was detrimental to cycling at 3.0 to 4.5 V operation voltages. Second we used X-ray diffraction and X-ray absorption to probe these reactions to better understand the mechanism of over-lithiation. It was found that a di-lithium Li_2NMCO_2 phase was formed, but the electrochemical reversibility is not adequate. Future experiments will evaluate other NMC classes for over-lithiated functionality.

References

W. M. Dose, M. J. Piernas-Munoz, V. A. Maroni, S. E. Trask, I. Bloom and C. S. Johnson, “Capacity fade in high-energy silicon-graphite electrodes for lithium-ion batteries”, Chem. Commun. (under revision)